Skoltech
Skolkovo Institute of Science and Technology

Jury Member Report – Doctor of Philosophy thesis.

Name of Candidate: Ilya Novikov

PhD Program: Materials Science and Engineering

Title of Thesis: Assembling networks of single-walled carbon nanotubes for electronic and optical applications

Supervisor: Professor Albert Nasibulin, Skoltech
Co-supervisors:
Professor Tanja Kallio, Aalto University
Assistant Professor Dmitry Krasnikov, Skoltech
Assistant Professor Fedor Fedorov, Skoltech

Name of the Reviewer:

I confirm the absence of any conflict of interest (Alternatively, Reviewer can formulate a possible conflict)	**Date: 05-09-2023**

The purpose of this report is to obtain an independent review from the members of PhD defense Jury before the thesis defense. The members of PhD defense Jury are asked to submit signed copy of the report at least 30 days prior the thesis defense. The Reviewers are asked to bring a copy of the completed report to the thesis defense and to discuss the contents of each report with each other before the thesis defense.

If the reviewers have any queries about the thesis which they wish to raise in advance, please contact the Chair of the Jury.

Reviewer's Report

Reviewers report should contain the following items:

- Brief evaluation of the thesis quality and overall structure of the dissertation.
- The relevance of the topic of dissertation work to its actual content
- The relevance of the methods used in the dissertation
- The scientific significance of the results obtained and their compliance with the international level and current state of the art
- The relevance of the obtained results to applications (if applicable)
- The quality of publications

The summary of issues to be addressed before/during the thesis defense

Overall, the candidate did a great job in summerising his work on FCCVD-based CNTs for potential optoelectrical applications. Here are some of the comments the candidate should address:

1. CO_2 and H_2 , the growth promoters and CO, the carbon source are all gases. Therefore, the ratio of the injected amounts of each component is important while they vary easily with even a small change in temperature. Because MFC (Mass Flow Controller) is a device that controls the flow rate per minute and at different temperatures, the number of molecules vary. Hence, how did you manage to maintain constant temperature? From the illustrations you provided there was no contraptions or equipment that help maintain the temperature.
2. Growth parameter, H_2 is recognised for their role in high yield and quality production of CNTs owing to their small size which give arise to high mobility and reactivity at high temperatures. As such, SWCNTs (single-walled carbon nanotubes) of higher yield and quality are typically synthesized at high temperatures only. Then, my question is that why CO exhibits optimal efficiency at a relatively low temperature of 880 'C. Alternatively, what results can we expect when the synthesis temperature is higher that 880 'C when using H2? If the optimal temperatures for the two promoters are different, more detailed explanation is called for.
3. In chapter 5, the candidate said the bundles get thicker from the SEM images (Fig 21), but it is difficult to agree from the provided images. (I highlighted it yellow. It would help a lot if you provide SWCNTs/bundles value over SWCNT/TPU nanocomposites)
4. Please check references. (I highlited them red) There seems to be a technical error
5. The graphs provided need to be improved greatly, especially the figure legends.
6. There are many grammar, unit, capital/small letter mistakes, commas, punctuality and so on. (I highlighted them blue)

Provisional Recommendation
☐ *I recommend that the candidate should defend the thesis by means of a formal thesis defense*
☒ *I recommend that the candidate should defend the thesis by means of a formal thesis defense only after appropriate changes would be introduced in candidate's thesis according to the recommendations of the present report*
☐ *The thesis is not acceptable and I recommend that the candidate be exempt from the formal thesis defense*

Chapter 5. Fabrication of SWCNT/polymer nanocomposites

5.1. Multifunctional elastic SWCNT/TPU nanocomposites

While SWCNT thin films as quasi-2D macroscale networks are applied mainly as TCFs, conductive SWCNT/polymer nanocomposites containing 3D nanotube networks are more functional because of polymer matrix. In particular, elastomer-based conductive nanocomposites are excellent material for soft lightweight stretchable and flexible electronics. Nevertheless, as discussed in Section 2.3.1, the crucial problem in nanocomposites is homogeneity of nanotube dispersion, which affects all the final properties of material. Spatial distribution of SWCNTs in SWCNT/TPU nanocomposites with different nanotube concentrations, which were manufactured by coagulation precipitation technique (CP) implying immediate nanocomposite formation, were estimated by SEM (**Figure 21**).
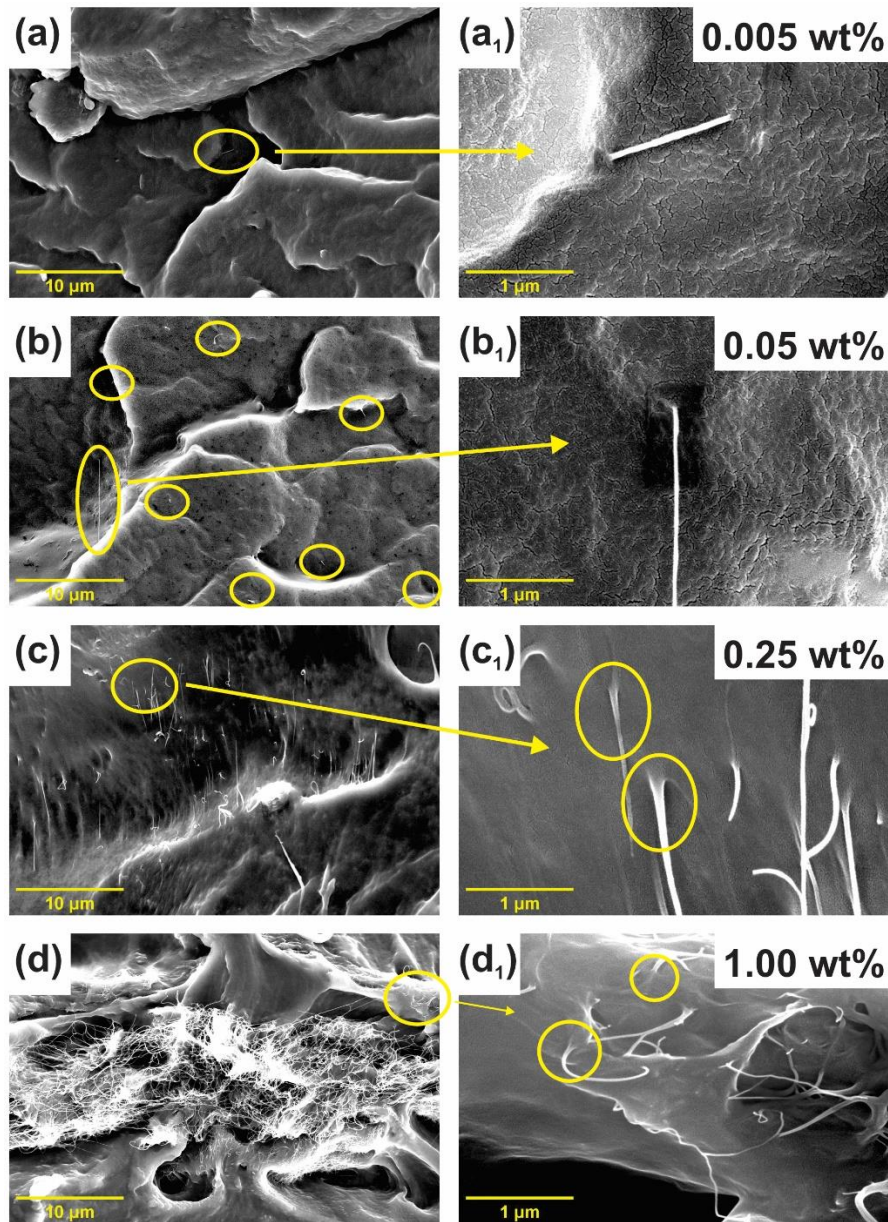
Figure 21. SEM images of fracture surface of SWCNT/TPU nanocomposites with different nanotube concentrations: **(a)** 0.005 wt%, **(b)** 0.05 wt%, **(c)** 0.25 wt%, **(d)** 1.00 wt%; yellow circles highlight SWCNTs/bundles enlarged in corresponding magnified images (a_1)-(d_1); yellow circles in the magnified images highlight nanotubes pullout off the polymer indicating high TPU wetting.

At the lowest concentration of 0.005 wt%, only individual SWCNTs/bundles randomly located in TPU matrix may be found. At the higher concentrations, uniform

SWCNT distribution can be observed until the highest concentrations (1.00 wt%) where 10-20 μm scale agglomerates are formed (**Figure 21d**). High dispersion degree is believed to be achieved by effective dispersion techniques (homogenization and ultrasonication) and quick nanocomposite formation by CP, although, at high nanotube loadings, dispersion is complicated by high suspension viscosity. Besides, magnified SEM images (**Figure 21c$_1$-d$_1$**) illustrate gradual thicking of bundles approaching TPU matrix, which might indicate high TPU wetting of nanotubes, which is attributed to high affinity of TPU to nanotubes and in the good agreement with the reported data [174,175]. Thus, SEM analysis reveals quite good prerequisites for nanocomposite properties achieved by high dispersion degree.

Nanocomposite conductivity was tested by impedance spectroscopy technique. conductivity-vs-frequency dependencies (Bode charts) for the nanocomposites with different nanotube loadings are shown in **Figure 22a**.
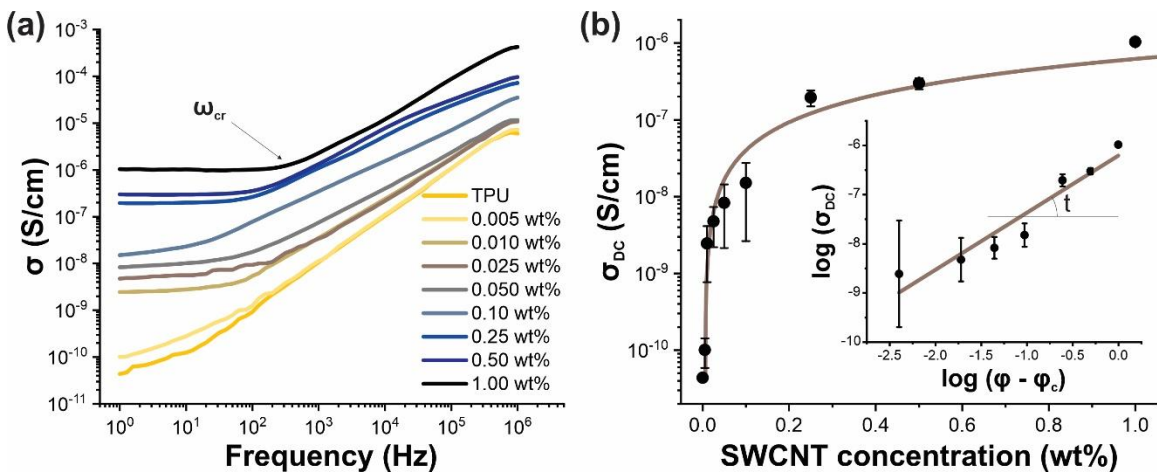
Figure 22. **(a)** Conductivity dependencies on frequency for SWCNT/nanotube nanocomposites with different concentrations (shown in legend) with highlighted critical frequency. **(b)** Dc conductivity plotted versus SWCNT concentration (percolation curve) with the same data plotted in log-log scales (inset) for determination of percolation threshold.

Impedance spectra demonstrate evident general increase in conductivity of nanocomposite with nanotube concentration. Meanwhile, two conductivity regimes can be identified in conductivity-vs-frequency curves: frequency-independent in the low-frequency region, and frequency dependent in the high-frequency one, which correlates with the other reported impedance results for nanocomposites [176,177]. Frequency-independent region indicates ohmic impedance response meaning nanotube-based conductive network is formed within TPU. Yet, the 0.005 wt%-concentrated nanocomposite does not demonstrate such a regime and essentially behaves identically to the pure TPU sample. Steady increase in conductivity with frequency reflects dielectric response to perturbating electromagnetic fields:

$$\sigma = \varepsilon_0 \varepsilon'' \omega, \tag{42}$$

where $\varepsilon_0 \cong 8.85$ F/m is vacuum permittivity, ε'' is imaginary dielectric permittivity and ω is frequency of applied field. This behavior is supported by the slope ~ 1.0 of the impedance curves.

Transition between two conductivity regions for higher-concentrated nanocomposites occurs at critical (characteristic) frequency ω_{cr} (indicated in **Figure 22a**). Below the transition, impedance response is determined by nanotube network, therefore, percolation threshold can be assumed in $0.005 - 0.010$ wt% concentration range. Meanwhile, with frequency increase, charge carrier travel distances, proportional to perturbating wavelength, decrease, reaching critical distance equal to an average inter-nanotube distance. Therefore, at higher distances, impedance is governed by capacitive

contribution and determined by insulating polymer wrapping nanotubes. This explains shift in ω_{cr} towards higher frequencies with SWCNT concentration increase.

Taken at the lowest frequency (1 Hz) applied, dc conductivity plotted versus SWCNT concentration represents a typical percolation curve (**Figure 22b**) described by equation (15). Since impedance spectra pointed to percolation threshold to be within 0.005 – 0.010 wt% range, iterative selection of percolation threshold φ_c in this range resulted in the best fitting at 0.006 wt% (inset in **Figure 22b**). Thus, an ultralow percolation threshold of 0.006 wt% was found which is orders of magnitude lower to the ones found for TPU-based nanocomposites prepared by CP [98] and is comparable to the lowest percolation thresholds reported (typically, for epoxy-based nanocomposites [87,90]). Moreover, according to equation (16) derived from percolation theory, for aspect ratio approximately equal to 3000 of nanotubes used, φ_c should be ~ 0.035 wt% (assuming SWCNT density as 1.9 g/cm^3). Considerably lower values found in conductivity measurements can be explained by kinetic nature of percolation threshold rather than statistical one. This implies flocculation between nanotubes leading to deviations from homogeneous distribution and formation of nanotube network within the whole host material at much lower concentrations [92].

Besides, the slope of the fitting line t (power value in equation (16)) could also provide some useful information of SWCNT network construction. Fitting results yield $t = 1.16 \pm 0.16$, which lower than 2.0 predicted for 3D SWCNT network conductivity governed by contact resistance. Decreased t values may be an indication of flocs in SWCNT network, which, although allow lower percolation, hinder scaling conductivity

with nanotube concentration, Yet, analysis of the parameter t is established as quite ambiguous and depends on many factors [87]. In addition, quite low conductivity values should be noted, which is likely attributed to dominance of tunnelling resistance contribution caused by high wetting of nanotubes by polyurethane.

Nevertheless, ultralow percolation threshold indicates a "golden middle" in the selection of aspect ratio of nanotubes and dispersion techniques. Quite moderate aspect ratio of ~ 3000 allows high dispersion degree, yet, at the same time, pretty long nanotubes construct percolative pathways at lower concentrations because of both, higher exclusive volume (in terms of percolation theory) and not very vigorous dispersion techniques allowing flocculation (moderate agglomeration) of nanotubes.

For estimation of applicability of nanocomposites in soft electronics, mechanical properties, in addition to electrical, should be evaluated too. Since these work touches on the conductivity topic, the results are given in short (detailed description of the results of tensile tests are presented in Publication II). Briefly, typical for nanocomposites, increase in elasticity (Young's modulus) and decrease in strain at break with SWCNT concentration was observed. These two trends lead to a maximum in tensile strength at 0.1 – 0.2 wt% concentration. Nevertheless, strain at break is generally maintained before 0.25 wt% (before significant agglomeration happened at the highest concentration as was found in SEM analysis (**Figure 21d**)) indicating that low-concentrated nanocomposites are of practical interest. Moreover, increase in Young's modulus related to nanotube amount added (from ~ 15 MPa to 30 MPa for 0.25 wt% concentration) appeared to be comparable or even superior to the results for CNT/polyurethane composites [98,124,125,178].

Simultaneous measurements of piezoresistive response of nanocomposites yielded highly promising results as well. Error! Reference source not found.**a** depicts stress-strain and corresponding $\Delta R/R_0$-strain curves in moderate strain range (250%), while Error! Reference source not found.**b** depicts the piezoresistive response in the whole strain range.
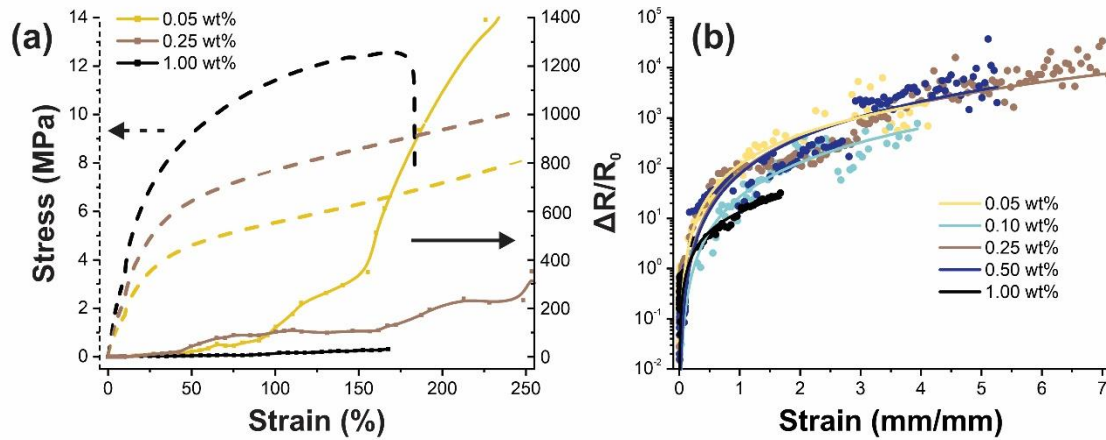
Figure 23. **(a)** Piezoresistive ($\Delta R/R_0$) response to strain (right y-axis) plotted with stress-strain curves (left y-axis) for SWCNT/TPU nanocomposites at 0.05, 025 and 1.00 wt% and **(b)** the same dependency plotted in the whole strain range.

Piezoresistive tests indicate decrease in mechanical sensitivity with nanotube concentration increase, which is in the good agreement with established mechanisms of composite strain sensing assuming the highest response at near-percolation threshold concentrations based on losses of contact junctions and exponential increase in tunnelling resistance (discussed in details in Section 2.3.1). Gauge factor (GF) values was calculated according to equation (17) in elastic range (since this deformation region allows multiple use of materials and is of practical interest; both are given in **Error! Reference source not found.**). Within the whole strain range, maximum GFs may be found (**Error! Reference source not found.**). The results point to the highest sensitivity for medium-concentrated

114

nanocomposites, which associated with, on the one hand, fast achievement of immeasurable resistances of GΩs for low-concentrated nanocomposites (which do not change at the following strain) and, on the other hand, brittleness of high-concentrated nanocomposites not allowing them to stretch sufficiently to reach breaks on nanotube network. Yet, GF in elastic region should be considered as a figure of merit. The very high GF value of 82 achieved at such low nanotube concentration of 0.05 wt% opens up extremely beneficial sides of nanocomposites proposed in this work: high performance at low concentrations. This result is reached because of ultralow percolation threshold.

Table 5. Elastic range and GF values determined for both elastic and the whole (maximum GF) strain ranges.

SWCNT concentration (wt%)	Elastic range (%)	GF in elastic range	Maximum GF
TPU	26	-	-
0.05	18	82 ± 2	480 ± 20
0.10	21	35 ± 2	150 ± 10
0.25	24	22 ± 9	1090 ± 30
0.50	21	15 ± 8	780 ± 30
1.00	22	8.0 ± 0.4	15.5 ± 1.8

This paradigm was achieved for EMI shielding efficiency in THz range too. **Figure 24a** represents transmittance spectra of SWCNT/TPU nanocomposites in THz range and **Figure 24b** shows resulting dependency of shielding efficiency normalized to the sample thickness dependency on SWCNT concentration at different probe frequencies. A steady drop in transmittance observed for all the nanocomposites corresponds to a typical for nanotube networks electrodynamic response explained within the framework of the Drude conductivity model (applicable for metals).
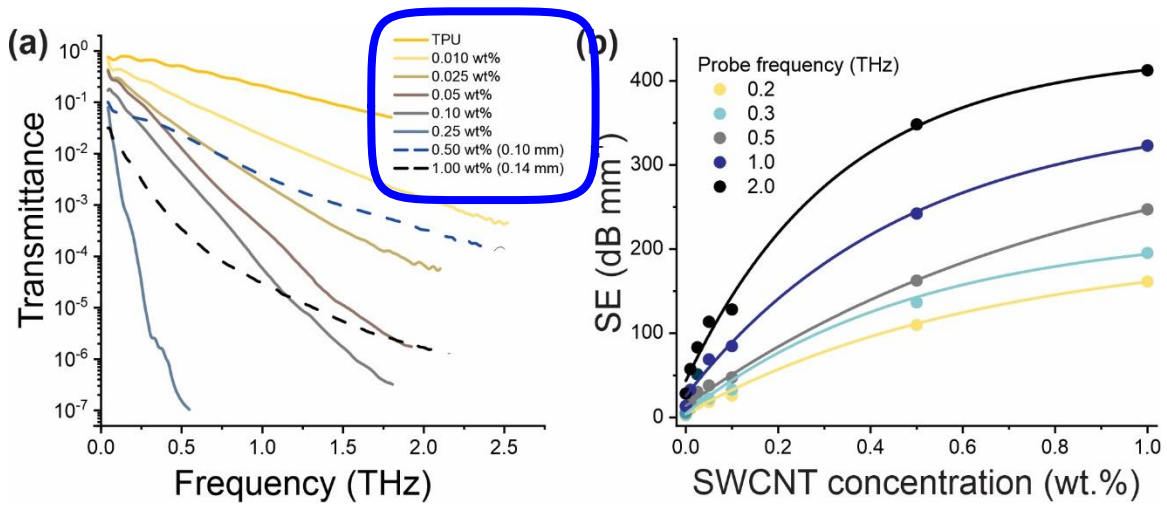
Figure 24. **(a)** Transmittance spectra of SWCNT/TPU nanocomposites with 0.5-mm thickness (unless the otherwise indicated) in THz range at different SWCNT concentration; **(b)** Normalized SE dependency on SWCNT concentration at different probe frequencies.

SWCNT/TPU nanocomposites exhibit extremely high shielding efficiency normalized to the sample thickness (calculated according to equation (30)), obviously growing with nanotube concentration. In particular, SE of 20 dB/mm at 1 THz frequency is achieved for very low concentration of 0.01 wt%, which supports the paradigm of high performance at low concentrations and originates from low percolation threshold.

The strain sensing and EMI shielding efficiency performance of SWCNT/TPU nanocomposites can be compared with the other reported results in these areas. State-of-the-art performance is noted for both GF and SE in THz range in terms of performance achieved at low concentrations (**Figure 25**). These remarkable results are attributed to the appropriate selection of SWCNT aspect ratio and nanocomposite manufacturing route (SWCNT dispersion and nanocomposite formation) yielding close-to-homogeneous spatial distribution of nanotubes, which allows formation of percolating pathways at ultralow concentrations, and provide great prospects for nanocomposite industry development.

116
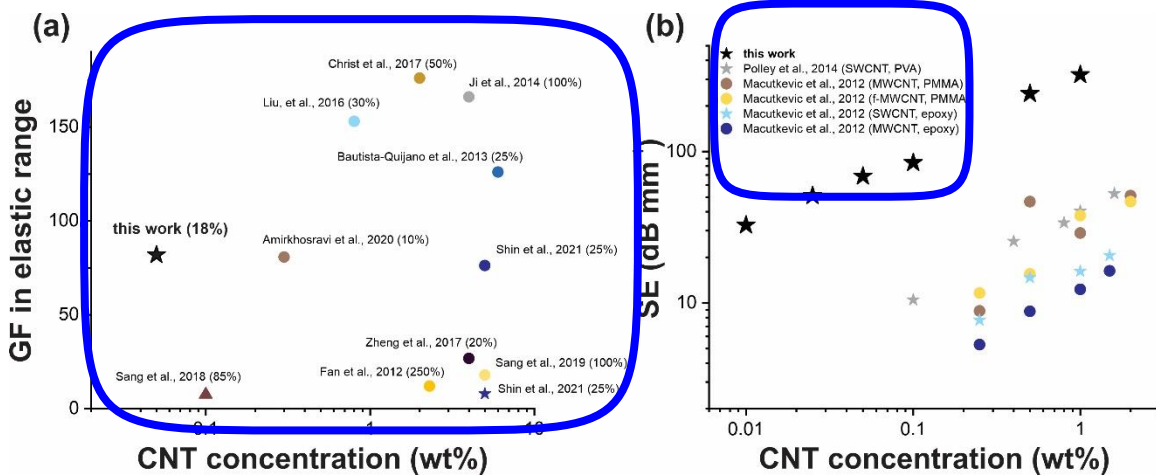
Figure 25. (a) The advances in the GF values plotted versus CNT concentration (strain is indicated in the brackets); ★ corresponds to SWCNTs, ● to MWCNTs, ▲ to carbon nanostructures based on MWCNTs. **(b)** The advances in the normalized SE values at 1 THz (CNT type and polymer are indicated in the brackets).

4.4. SWCNT/thermoset nanocomposites. Nanotube bulk density optimization.

As was discussed above, nanotube dispersion is the primary problem in CNT/polymer nanocomposite manufacturing. Commercial masterbatches (MBs) is one of the most convenient solutions of this problem for industry. Highly-concentrated pastes with pre-dispersed nanotubes can be easily incorporated in manufacturing process and do not require specific equipment necessary for CNT powder processing. Densely packed in polymer, CNTs cannot be aerosolized, which significantly lowers health risks. Nevertheless, MBs possess certain drawbacks: specificity to certain polymers, specific storage conditions, and high price compared to raw nanotube powders.

Briquettes, fabrication procedure of which is described in Section 2.3.2, are alternative polymer-unspecific solution. Nevertheless, compression of nanotubes could affect their subsequent dispersion in polymer (for instance, leads to an increase

117

agglomeration/entanglement degree) or introduce defects in SWCNT structure. BET analysis and Raman spectroscopy results indicated no noticeable changes caused by both compression and rapid expansion (RESS) of nanotube powders (**Table 1**). Nanotube agglomeration state in the scale of tens of microns also seems unchanged according to the SEM observations (**Figure 26c-e**). However, bulk density of the powder varies in orders of magnitude (**Table 1**, powders are captured and illustrated in **Figure 26a-b**)
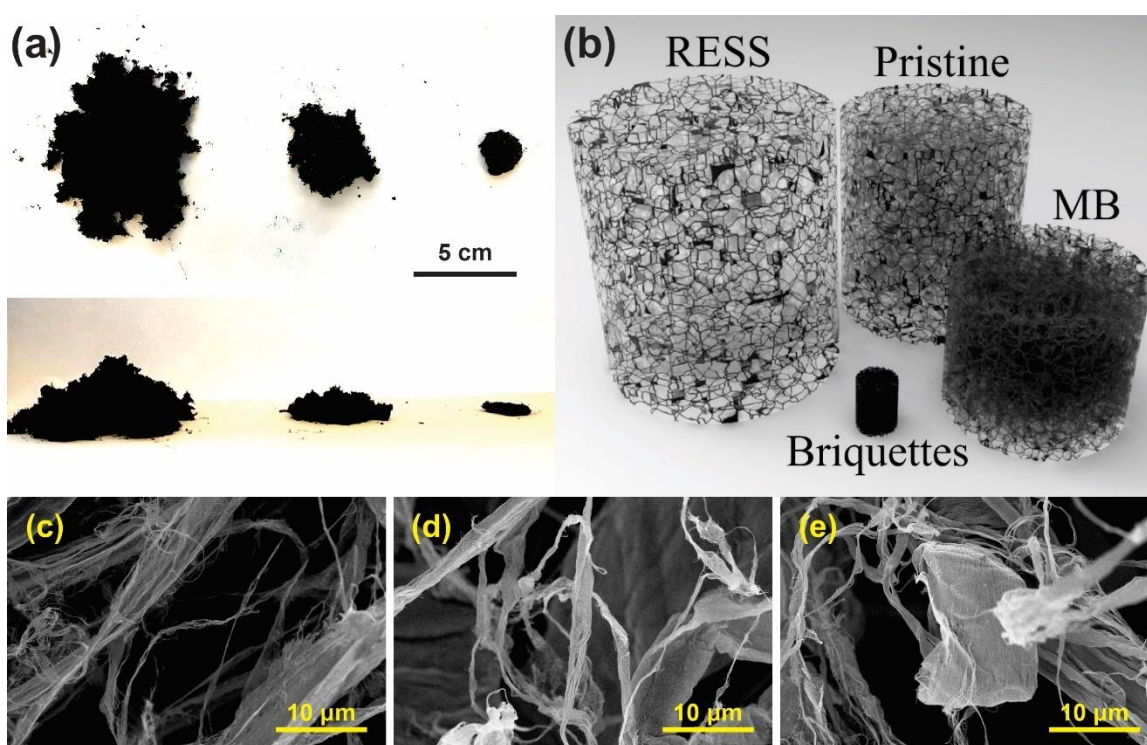
Figure 26. **(a)** Photos of SWCNT powder types (from left to right: RESS, pristine, briquettes) from top view (top) and side view (bottom). **(b)** Schematic representation of differences in bulk densities of nanotubes of different type. SEM images of **(c)** RESS, **(d)** pristine, and **(e)** briquette types of SWCNTs.

Thus, with the exception of bulk densities (where briquettes possess evident advantages for the practical use), all the other initial parameters of SWCNTs are the same. SEM analysis of SWCNT/epoxy nanocomposites fabricated from these three types of

SWCNT powders and MBs (four types total) also did not yield noticeable differences between nanotube morphology (images in Publication III). At the lowest concentrations, in all four types of nanocomposites, SWNCTs tend to form small agglomerates of bundles/nanotubes widely and unformly distributed in epoxy matrix. Reaching higher concentrations, distances between these agglomerates decrease, while their size, on contrary, increases, until, at the highest concentrations (~ 1.00 wt%) all the observed area of nanocomposite fracture surface contains interconnected SWCNT network. Thus, since nanotube morphology governs the resulting properties of nanocomposites, those prepared from nanotube briquettes have prerequisites to perform in similar manner despite huge variations of bulk density of raw nanotube material.

Both dc and ac conductivity tests were carried out for nanocomposites. Percolation curves obtained are demonstrated in **Figure 27a** (dc and ac measurements gave identical results (SI in Publication III).
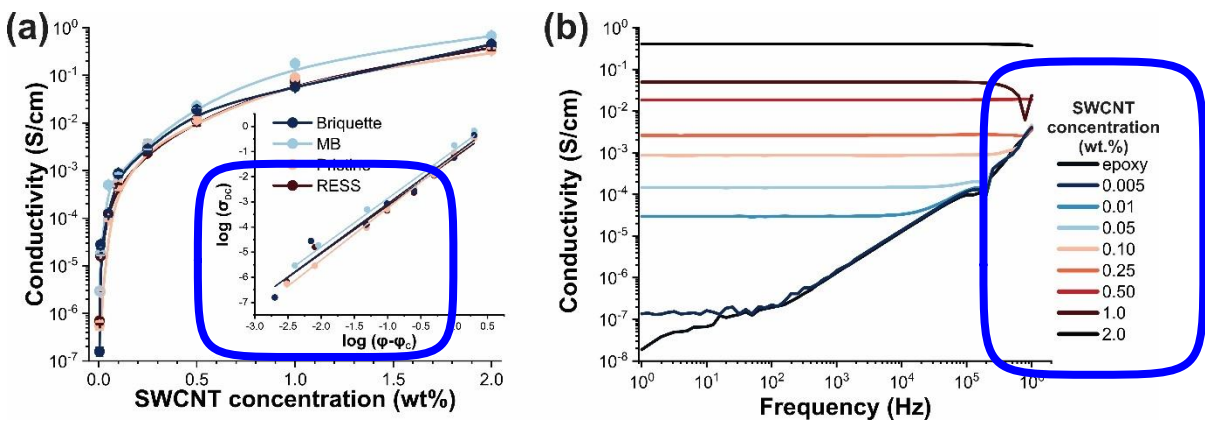
Figure 27. (a) Percolation curves (conductivity-vs-nanotube concentration) obtained for different type of nanocomposites (indicated in legend) and the same data plotted in log-log scales (inset). **(b)** Impedance spectra of pristine SWCNT/epoxy nanocomposites with different nanotube concentration.

Compared to SWCNT/TPU nanocomposites, SWCNT/epoxy ones demonstrate much higher conductivity (reaching 10^{-1} S/cm for 1.0 wt%). It could be explained by absence of polymer wettability observed for TPU, which is also supported by SEM (Publication III). **Table 6** contains the results of percolation threshold determination and exponential parameter t (from equation (15)).

Table 6. Percolation thresholds and scaling parameter t found for different types of SWCNT/epoxy nanocomposites.

Series	φ_c (wt%)	t
Briquettes	0.003	1.94 ± 0.14
MB	0.001	1.92 ± 0.09
Pristine	0.002	2.07 ± 0.04
RESS	0.002	1.90 ± 0.10

All the nanocomposites have ultra-low percolation thresholds, meanwhile, the deviations between different types are insignificant. Such a low values should be attributed to manufacturing technique and moderate SWCNT aspect ratio (as it was discussed for SWCNT/TPU nanocomposites). Nevertheless, in contrast to the TPU-based ones, scaling parameter t of SWCNT/epoxy nanocomposite appeared to be noticeably higher, around 2.0, which is in excellent correlation with percolation theory [87].

To investigate features of nanocomposite conductivity behavior, we utilized impedance spectroscopy (as it was done for TPU nanocomposites, **Figure 27b**). Curiously, impedance response turned out to be different compared to polyurethane-based samples. In this case, pronounced, frequency-independent region is observed for all the SWCNT concentrations, including the lowest 0.005 wt% (obviously, with the exception of pure polymer), meaning percolation thresholds to be lower than 0.005 wt%, this way verifying

120

the results obtained from dc conductivity analysis. Moreover, above 0.25 wt%, within 1 Hz – 1 MHz frequency range studied, no frequency-dependent regions can be revealed at all. This implies that average inter-tube distance corresponding to the characteristic (critical) frequency is not achieved indicating higher SWCNT dispersion degree than it was achieved for TPU nanocomposites. This assumption is supported by lower percolation thresholds too. Nonetheless, as the same as for the TPU nanocomposites nanotubes were used (commercial SWCNTs with ~ 3000 aspect ratio), they are considerably lower the theoretically predicted value, which also points to flocculation structure in nanotube network.

Thus, SWCNT/epoxy nanocomposites demonstrate remarkable electrical conductivity properties with both ultralow percolation thresholds (0.001 – 0.003 wt%) and, unlike TPU/SWCNT nanocomposites, high conductivity (~ 10^{-1} S/cm for 1.0 wt%). Meanwhile, densely packed SWCNT briquettes used as an initial material resulted in the similarly high conductivity as the other samples, including ones based on commercial MBs.

In addition to electrical conductivity tests, the nanocomposites were tested on thermal conductivity and stability. These parameters appeared to be similar too (details are in Publication III), which supports the identity of the nanocomposites fabricated from SWCNT powders with different bulk density (consolidation degree). This is caused by similar nanotube morphology in polymer, which, in turn, is likely come from similar properties of raw powders (defectiveness, surface area, morphology). Apparently, compression procedure, which increase bulk density by more than 20 times, affects

macroscale nanotube organization, while the microscale one (determining the properties) is left unchanged.

Briquette-packed SWCNT powders provide a highly promising solution for nanocomposite industry, since they are significantly simpler for processing compared to pristine powders, but noticeably cheaper and not polymer-specific as MBs. These advantages are illustrated in **Figure 28**.
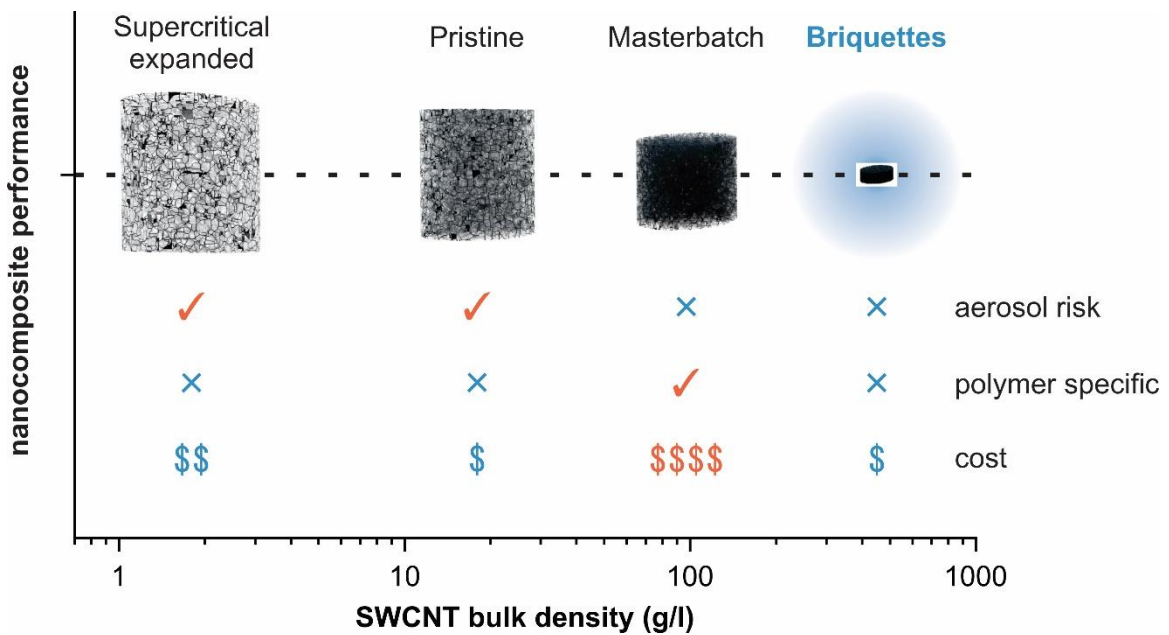
Figure 28. Schematic illustration of briquette-packed SWCNT powders providing identical nanocomposite performance than the other types of raw SWCNT material but, because of much higher bulk density, being advantageous over the rest ones.

Chapter 6. Conclusions

The current thesis addresses the problems of controllable assembling of SWCNT networks in macromaterials for their subsequent employment in electronic and optical applications. Meanwhile, two branches of the study were formulated. The first one concerns the controlled synthesis of quasi-2D nanotube networks – thin SWCNT films, which main application is transparent conductive films. The second direction is devoted to the problems of SWCNT organization in 3D network in host polymer – nanocomposite formation, which conductivity properties were realized in such applications as mechanical sensing (piezoresistivity) and shielding from electromagnetic fields.

Within the framework of the work devoted to the production of TCFs based on SWCNTs, CO-based aerosol CVD method for nanotube synthesis was utilized and adjusted. Chemical engineering of the reactor was fulfilled for improvement of figure of merits of the product (film conductivity, or, R_{90}) and the process (synthesis productivity, or, yield).

Firstly, investigation related to the controllable tuning of residence time was conducted. Herewith, the key aspect was to keep the first stage of nanotube synthesis – catalyst activation – unchanged when residence time is varied. Extension in residence time led to nanotube lengthening, while nanotube diameter distribution was maintained, which indicated maintained catalyst activation. Controllable nanotube lengthening resulted in the considerable decrease in R_{90}. Tis strategy coupled with optimized synthesis conditions and doping resulted in R_{90} of 51 Ω/□.

Next step in development of aerosol CVD process involved introduction of hydrogen as a reducing growth promoter, poorly studied in CO-process before. Addition of H_2 resulted in significant increase in synthesis productivity caused by appearance of new carbon-feeding reaction between CO and H_2. Meanwhile, different H_2 effects were found depending on a temperature regime used, which was associated with different nanotube growth rate-limiting stages. In the low-T regime (880 °C), yield was remarkably increased by 15 times at the maintained film conductivity, while in the high-T one (1000 °C), hydrogen affect positively both yield and film conductivity, which was achieved by nanotube lengthening.

The developed method based on controllable tuning of residence time allowed consideration the crucial problem in aerosol CVD process – reactor scaling which requires evaluation of nanotube growth kinetics. Assessment of growth rate and catalyst lifetime appeared to be possible by analyzing R_{90} versus residence time trends, which correlation with length was demonstrated and proved. Such method is considerably simpler than reactor scaling followed by routine measurements of nanotube length collected at different residence times. In particular, it was utilized for investigation of CO_2 (oxidative growth promoter) effect on catalyst deactivation rate. It was revealed that CO_2 accelerates nanotube growth but causes faster catalyst deactivation.

Besides, a new approach to optimization of SWCNT performance as TCFs based on fabricating SWCNT films with a rational design – patterning – was proposed. This one-stage and liquid-free method is based on thermal sputtering of metal onto the filter through a patterned mask and the use of such filter-mask for selective filtration of aerosol SWCNT

124

flow. Deposited nanotubes form mesh-shaped patterned film, which equivalent sheet resistance is 2-3 times lower than that of continuous film. With applying doping procedure in addition to patterning, about 12-fold decrease in R_0 (from ~ 1 kΩ/□ to 90 Ω/□) was reached.

Approaches to assembling 3D SWCNT networks in polymers were proposed with purpose on optimization of conductivity as well, in this case, of nanocomposites. Meanwhile, here, commercial SWCNTs with moderate (~ 3000) aspect ratio were used as a starting raw material.

First, fabrication of elastic SWCNT/polymer nanocomposites as an excellent material for stretchable and flexible soft electronic devices was studied. In this work, TPU was utilized as an elastomer and rarely employed coagulation precipitation technique assuming immediate SWCNT/polymer nanocomposite formation was used. Fabrication approaches resulted in close-to-uniform SWCNT dispersion degree in polyurethane confirmed by SEM which resulted in the ultralow percolation threshold of 0.006 wt%. and opened great opportunities for conductivity-based application of SWCNT/TPU elastic nanocomposites. Sensitivity to mechanical strains was characterized by gauge factor of 82 at 0.05 wt% nanotube concentration, while EMI shielding efficiency was found to be 20 dB for 1-mm thick sample at 1 THz. Thus, high performance of nanocomposites was achieved at very low SWCNT concentrations, which propose great economic prospects for nanocomposite industry.

Another potentially useful for nanocomposite industry study was devoted to optimization of SWCNT powder packaging for simplification of manufacturing

procedures. Densely packed (bulk density of 450 g/l) briquette-shaped SWNCT powders (prepared from pristine ones with bulk density of 19 g/l) were proposed as a polymer-unspecific and cheap alternative to currently existing MBs used for simple nanocomposite fabrication. To assess nanotube compression (consolidation) effect, SWCNT/epoxy (thermoset) nanocomposites fabricated from briquettes were compared to the similar one produced from pristine and expanded nanotube powders, as well as from MBs. Surprisingly, SEM analysis and electrical conductivity behavior appeared to be identical for all four types of nanocomposites. Moreover, ultralow percolation thresholds (0.001 – 0.003 wt%) were reached again, however, in contrast to SWCNT/TPU nanocomposites, maximum conductivity was significantly higher (~ 0.1 S/cm for 1.0 wt% concentration).

Summing up, the significant improvement in conductivity of SWCNT network-based thin films and nanocomposites was achieved, which reveals great prospects for industrial applications. The mechanisms behind these improvements were thoroughly investigated and discussed. New approaches proposed and developed within the framework of the current theses could be useful both for academia and industry.

Bibliography

[1]   Radushkevich LV, Lukyanovich VM, O strukture ugleroda, obrazujucegosja pri termiceskom razlozenii okisi ugleroda na zeleznom kontakte, Zurn Fisic Chim 26 (1952) 88–95.

[2]   A. Oberlin, M. Endo, T. Koyama, Filamentous growth of carbon through benzene decomposition, J Cryst Grpwth. 32 (1976) 335-349. https://doi.org/10.1016/0022-0248(76)90115-9.

[3]   S. Iijima, Helical microtubules of graphite carbon, Nature. 354 (1991) 56-58. http://dx.doi.org/10.1038/354056a0.

[4]   H. Chen, A. Roy, J.B. Baek, L. Zhu, J. Qu, L. Dai, Controlled growth and modification of vertically-aligned carbon nanotubes for multifunctional applications, Materials Science and Engineering R: Reports. 70 (2010) 63–91. https://doi.org/10.1016/j.mser.2010.06.003.

[5]   E. Theocharous, C.J. Chunnilall, R. Mole, D. Gibbs, N. Fox, N. Shang, G. Howlett, B. Jensen, R. Taylor, J.R. Reveles, O.B. Harris, N. Ahmed, The partial space qualification of a vertically aligned carbon nanotube coating on aluminium substrates for EO applications, Opt Express. 22 (2014) 7290. https://doi.org/10.1364/oe.22.007290.

[6]   E.T. Thostenson, W.Z. Li, D.Z. Wang, Z.F. Ren, T.W. Chou, Carbon nanotube/carbon fiber hybrid multiscale composites, J Appl Phys. 91 (2002) 6034–6037. https://doi.org/10.1063/1.1466880.

[7]   N. Behabtu, C.C. Young, D.E. Tsentalovich, O. Kleinerman, X. Wang, A.W.K. Ma, E. Amram Bengio, R.F. Ter Waarbeek, J.J. De Jong, R.E. Hoogerwerf, S.B. Fairchild, J.B. Ferguson, B. Maruyama, J. Kono, Y. Talmon, Y. Cohen, M.J. Otto, M. Pasquali, Strong, Light, Multifunctional Fibers of Carbon Nanotubes with Ultrahigh Conductivity, Science. 339 (2013) 182-186. https://doi.org/10.1126/science.1228061.

[8]   W. Yang, P. Thordarson, J.J. Gooding, S.P. Ringer, F. Braet, Carbon nanotubes for biological and biomedical applications, Nanotechnology. 18 (2007) 412001. https://doi.org/10.1088/0957-4484/18/41/412001.

[9]   E.A. Laird, F. Kuemmeth, G.A. Steele, K. Grove-Rasmussen, J. Nygård, K. Flensberg, L.P. Kouwenhoven, Quantum transport in carbon nanotubes, Rev Mod Phys. 87 (2015) 703-764. https://doi.org/10.1103/RevModPhys.87.703.

[10]   A.K. Geim, K.S. Novoselov, The rise of graphene. Nature Mater. 6 (2007) 183-191. https://doi.org/10.1038/nmat1849

[11]   M.S. Dresselhaus, G. Dresselhaus, R. Saito, Physics of carbon nanotubes. 33 (1995) 883-891. https://doi.org/10.1016/0008-6223(95)00017-8.

[12]   J.W. Mintmire, C.T. White, Electronic and structural properties of carbon nanotubes, Carbon Nanotubes. (1996) 37–46. https://doi.org/10.1016/b978-0-08-042682-2.50010-2.

[13]   J. Wilder, L. Venema, A. Rinzler, R.E. Smalley, C. Dekker. Electronic structure of atomically resolved carbon nanotubes. Nature 391 (1998) 59–62. https://doi.org/10.1038/34139.

[14]   R. Saito, M. Fujita, G. Dresselhaus, M.S. Dresselhaus, Electronic structure of chiral graphene tubules, Appl Phys Lett. 60 (1992) 2204–2206. https://doi.org/10.1063/1.107080.

[15]   H. Kataura A, Y. Kumazawa, Y. Maniwa, I. Umezu, S. Suzuki, Y. Ohtsuka, Y. Achiba, Optical Properties of Single-Wall Carbon Nanotubes. Synth Metals 103 (1999) 2555-2558. https://doi.org/10.1016/S0379-6779(98)00278-1.

[16]   Alamusi, N. Hu, H. Fukunaga, S. Atobe, Y. Liu, J. Li, Piezoresistive strain sensors made from carbon nanotubes based polymer nanocomposites, Sensors. 11 (2011) 10691–10723. https://doi.org/10.3390/s111110691.

[17]   W. Obitayo, T. Liu, A review: Carbon nanotube-based piezoresistive strain sensors, J Sens. 2012 (2012). https://doi.org/10.1155/2012/652438.

[18]   F. Du, J.E. Fischer, K.I. Winey, Effect of nanotube alignment on percolation conductivity in carbon nanotube/polymer composites, Phys Rev B Condens Matter Mater Phys. 72 (2005) 121404. https://doi.org/10.1103/PhysRevB.72.121404.

[19]   F. Yang, M. Wang, D. Zhang, J. Yang, M. Zheng, Y. Li, Chirality Pure Carbon Nanotubes: Growth, Sorting, and Characterization, Chem Rev. 120 (2020) 2693–2758. https://doi.org/10.1021/acs.chemrev.9b00835.

[20]   L. Yu, C. Shearer, J. Shapter, Recent Development of Carbon Nanotube Transparent Conductive Films, Chem Rev. 116 (2016) 13413–13453. https://doi.org/10.1021/acs.chemrev.6b00179.

[21]   H. Geng, K. Kang Kim, K. Lee, G. Yong Kim, H. Kyu Choi, D. Sik Lee, K.A. Hyeok, Y. Hee Lee, Y. Chang, Y. Sil Lee, B. Kim, Y. Jun Lee, Depedenence of material quality on performance of flexible transparent conducting films with single-walled carbon nanotubes, Nano. 2 (2007) 157-167. https://doi.org/10.1142/S1793292007000532

[22]   M. S. Fuhrer, J. Nygård, L. Shih, M. Forero, Young-Gui Yoon, M. S. C. Mazzoni, Hyoung Joon Choi, Jisoon Ihm, Steven G. Louie, A. Zettl, and Paul L. McEuen. Crossed Nanotube Junctions, Science. 288 (200) 494-497. https://doi.org/10.1126/science.288.5465.494

[23]   M.A. Topinka, M.W. Rowell, D. Goldhaber-Gordon, M.D. McGehee, D.S. Hecht, G. Gruner, Charge transport in interpenetrating networks of semiconducting and metallic carbon nanotubes, Nano Lett. 9 (2009) 1866–1871. https://doi.org/10.1021/nl803849e.

[24] K. Yanagi, H. Udoguchi, S. Sagitani, Y. Oshima, T. Takenobu, H. Kataura, T. Ishida, K. Matsuda, Y. Maniwa, Transport mechanisms in metallic and semiconducting single-wall carbon nanotube networks, ACS Nano. 4 (2010) 4027–4032. https://doi.org/10.1021/nn101177n.

[25] R.K. Jackson, A. Munro, K. Nebesny, N. Armstrong, S. Graham, Evaluation of transparent carbon nanotube networks of homogeneous electronic type, ACS Nano. 4 (2010) 1377–1384. https://doi.org/10.1021/nn9010076.

[26] K.K. Kim, J.J. Bae, H.K. Park, S.M. Kim, H.-Z. Geng, K.A. Park, H.-J. Shin, S.-M. Yoon, A. Benayad, J.-Y. Choi, Y.H. Lee, Fermi level engineering of single-walled carbon nanotubes by AuCl3 doping., J Am Chem Soc. 130 (2008) 12757–12761. https://doi.org/10.1021/ja8038689.

[27] A. Znidarsic, A. Kaskela, P. Laiho, M. Gaberscek, Y. Ohno, A.G. Nasibulin, E.I. Kauppinen, A. Hassanien, Spatially resolved transport properties of pristine and doped single-walled carbon nanotube networks, Journal of Physical Chemistry C. 117 (2013) 13324–13330. https://doi.org/10.1021/jp403983y.

[28] D. Hecht, L. Hu, G. Grüner, Conductivity scaling with bundle length and diameter in single walled carbon nanotube networks, Appl Phys Lett. 89 (2006) 1–4. https://doi.org/10.1063/1.2356999.

[29] E.M. Khabushev, D.V. Krasnikov, J. V. Kolodiazhnaia, A.V. Bubis, A.G. Nasibulin, Structure-dependent performance of single-walled carbon nanotube films in transparent and conductive applications, Carbon. 161 (2020) 712–717. https://doi.org/10.1016/j.carbon.2020.01.068.

[30] A.G. Nasibulin, A. Ollikainen, A.S. Anisimov, D.P. Brown, P. V. Pikhitsa, S. Holopainen, J.S. Penttilä, P. Helistö, J. Ruokolainen, M. Choi, E.I. Kauppinen, Integration of single-walled carbon nanotubes into polymer films by thermo-compression, Chemical Engineering Journal. 136 (2008) 409–413. https://doi.org/10.1016/j.cej.2007.04.033.

[31] G.A. Ermolaev, A.P. Tsapenko, V.S. Volkov, A.S. Anisimov, Y.G. Gladush, A.G. Nasibulin, Express determination of thickness and dielectric function of single-walled carbon nanotube films, Appl Phys Lett. 116 (2020). https://doi.org/10.1063/5.0012933.

[32] L. Zhao, S. Yu, J. Li, M. Wu, L. Li, X. Wang, Highly reliable flexible transparent conductors prepared with Cu/Ni grid by vacuum-free solution process, Opt Mater (Amst). 120 (2021) 111427. https://doi.org/10.1016/j.optmat.2021.111427.

[33] W. He, C. Ye, Flexible Transparent Conductive Films on the Basis of Ag Nanowires: Design and Applications: A Review, J Mater Sci Technol. 31 (2015) 581–588. https://doi.org/10.1016/j.jmst.2014.11.020.

[34] P.C. Wang, L.H. Liu, D. Alemu Mengistie, K.H. Li, B.J. Wen, T.S. Liu, C.W. Chu, Transparent electrodes based on conducting polymers for display

applications, Displays. 34 (2013) 301–314.
https://doi.org/10.1016/j.displa.2013.05.003.

[35]   D.J. Lipomi, J.A. Lee, M. Vosgueritchian, B.C.K. Tee, J.A. Bolander, Z. Bao, Electronic properties of transparent conductive films of PEDOT:PSS on stretchable substrates, Chemistry of Materials. 24 (2012) 373–382. https://doi.org/10.1021/cm203216m.

[36]   C. Bulumulla, R. Gunawardhana, P.L. Gamage, J.T. Miller, R.N. Kularatne, M.C. Biewer, M.C. Stefan, Pyrrole-Containing Semiconducting Materials: Synthesis and Applications in Organic Photovoltaics and Organic Field-Effect Transistors, ACS Appl Mater Interfaces. 12 (2020) 32209–32232. https://doi.org/10.1021/acsami.0c07161.

[37]   W. Greenbank, L. Hirsch, G. Wantz, S. Chambon, Interfacial thermal degradation in inverted organic solar cells, Appl Phys Lett. 107 (2015). https://doi.org/10.1063/1.4938554.

[38]   M. Trchová, I. Šeděnková, Z. Morávková, J. Stejskal, Conducting polymer and ionic liquid: Improved thermal stability of the material - A spectroscopic study, Polym Degrad Stab. 109 (2014) 27–32. https://doi.org/10.1016/j.polymdegradstab.2014.06.012.

[39]   Q. Zheng, Z. Li, J. Yang, J.K. Kim, Graphene oxide-based transparent conductive films, Prog Mater Sci. 64 (2014) 200–247. https://doi.org/10.1016/j.pmatsci.2014.03.004.

[40]   X. Li, Y. Zhu, W. Cai, M. Borysiak, B. Han, D. Chen, R.D. Piner, L. Colomba, R.S. Ruoff, Transfer of large-area graphene films for high-performance transparent conductive electrodes, Nano Lett. 9 (2009) 4359–4363. https://doi.org/10.1021/nl902623y.

[41]   D.A. Ilatovskii, E.P. Gilshtein, O.E. Glukhova, A.G. Nasibulin, Transparent Conducting Films Based on Carbon Nanotubes: Rational Design toward the Theoretical Limit, Advanced Science. 9 (2022) 2201673. https://doi.org/10.1002/advs.202201673.

[42]   D.W. Shin, J.H. Lee, Y.H. Kim, S.M. Yu, S.Y. Park, J.B. Yoo, A role of HNO3 on transparent conducting film with single-walled carbon nanotubes, Nanotechnology. 20 (2009). https://doi.org/10.1088/0957-4484/20/47/475703.

[43]   A.P. Tsapenko, A.E. Goldt, E. Shulga, Z.I. Popov, K.I. Maslakov, A.S. Anisimov, P.B. Sorokin, A.G. Nasibulin, Highly conductive and transparent films of HAuCl4-doped single-walled carbon nanotubes for flexible applications, Carbon N Y. 130 (2018) 448–457. https://doi.org/10.1016/j.carbon.2018.01.016.

[44]   O.T. Zaremba, A.E. Goldt, E.M. Khabushev, A.S. Anisimov, A.G. Nasibulin, Highly efficient doping of carbon nanotube films with chloroauric acid by dip-coating, Mater Sci Eng B Solid State Mater Adv Technol. 278 (2022). https://doi.org/10.1016/j.mseb.2022.115648.

130

[45]   A.E. Goldt, O.T. Zaremba, M.O. Bulavskiy, F.S. Fedorov, K. V. Larionov, A.P. Tsapenko, Z.I. Popov, P. Sorokin, A.S. Anisimov, H. Inani, J. Kotakoski, K. Mustonen, A.G. Nasibulin, Highly efficient bilateral doping of single-walled carbon nanotubes, J Mater Chem C Mater. 9 (2021) 4514–4521. https://doi.org/10.1039/d0tc05996j.

[46]   D.S. Kopylova, D.A. Satco, E.M. Khabushev, A. V. Bubis, D. V. Krasnikov, T. Kallio, A.G. Nasibulin, Electrochemical enhancement of optoelectronic performance of transparent and conducting single-walled carbon nanotube films, Carbon N Y. 167 (2020) 244–248. https://doi.org/10.1016/j.carbon.2020.05.103.

[47]   E.M. Khabushev, D.V. Krasnikov, O.T. Zaremba, A.P. Tsapenko, A.E. Goldt, A.G. Nasibulin, Machine Learning for Tailoring Optoelectronic Properties of Single-Walled Carbon Nanotube Films, Journal of Physical Chemistry Letters. (2019) 6962–6966. https://doi.org/10.1021/acs.jpclett.9b02777.

[48]   I.V. Novikov, E.M. Khabushev, D.V. Krasnikov, A.V. Bubis, A.E. Goldt, S.D. Shandakov, A.G. Nasibulin, Residence time effect on single-walled carbon nanotube synthesis in an aerosol CVD reactor, Chemical Engineering Journal. 420 (2021) 129869. https://doi.org/10.1016/j.cej.2021.129869.

[49]   N. Fukaya, D.Y. Kim, S. Kishimoto, S. Noda, Y. Ohno, One-step sub-10 μm patterning of carbon-nanotube thin films for transparent conductor applications, ACS Nano. 8 (2014) 3285–3293. https://doi.org/10.1021/nn4041975.

[50]   D. Mitin, Y. Berdnikov, A. Vorobyev, A. Mozharov, S. Raudik, O. Koval, V. Neplokh, E. Moiseev, D. Ilatovskii, A.G. Nasibulin, I. Mukhin, Optimization of Optoelectronic Properties of Patterned Single-Walled Carbon Nanotube Films, ACS Appl Mater Interfaces. 12 (2020) 55141–55147. https://doi.org/10.1021/acsami.0c14783.

[51]   V. Jourdain, C. Bichara, Current understanding of the growth of carbon nanotubes in catalytic chemical vapour deposition, Carbon. 58 (2013) 2–39. https://doi.org/10.1016/j.carbon.2013.02.046.

[52]   Q. Wen, R. Zhang, W. Qian, Y. Wang, P. Tan, J. Nie, F. Wei, Growing 20 cm long DWNTs/TWNTs at a rapid growth rate of 80-90 μm/s, Chemistry of Materials. 22 (2010) 1294–1296. https://doi.org/10.1021/cm903866z.

[53]   H.M. Cheng, F. Li, G. Su, H.Y. Pan, L.L. He, X. Sun, M.S. Dresselhaus, Large-scale and low-cost synthesis of single-walled carbon nanotubes by the catalytic pyrolysis of hydrocarbons, Appl Phys Lett. 72 (1998) 3282–3284. https://doi.org/10.1063/1.121624.

[54]   F. Smail, A. Boies, A. Windle, Direct spinning of CNT fibres: Past, present and future scale up, Carbon N Y. 152 (2019) 218–232. https://doi.org/10.1016/j.carbon.2019.05.024.

[55] A.G. Nasibulin, A. Moisala, D.P. Brown, H. Jiang, E.I. Kauppinen, A novel aerosol method for single walled carbon nanotube synthesis, Chem Phys Lett. 402 (2005) 227–232. https://doi.org/10.1016/j.cplett.2004.12.040.

[56] J.S. Bulmer, A.W.N. Sloan, M. Glerum, J. Carpena-Núñez, R. Waelder, J. Humes, A.M. Boies, M. Pasquali, R. Rao, B. Maruyama, Forecasting carbon nanotube diameter in floating catalyst chemical vapor deposition, Carbon N Y. 201 (2023) 719–733. https://doi.org/10.1016/j.carbon.2022.08.001.

[57] L. Weller, F.R. Smail, J.A. Elliott, A.H. Windle, A.M. Boies, S. Hochgreb, Mapping the parameter space for direct-spun carbon nanotube aerogels, Carbon N Y. 146 (2019) 789–812. https://doi.org/10.1016/j.carbon.2019.01.091.

[58] W. Tan, J.C. Stallard, F.R. Smail, A.M. Boies, N.A. Fleck, The mechanical and electrical properties of direct-spun carbon nanotube mat-epoxy composites, Carbon N Y. 150 (2019) 489–504. https://doi.org/10.1016/j.carbon.2019.04.118.

[59] A. Kaskela, A.G. Nasibulin, M.Y. Timmermans, B. Aitchison, A. Papadimitratos, Y. Tian, Z. Zhu, H. Jiang, D.P. Brown, A. Zakhidov, E.I. Kauppinen, Aerosol-synthesized SWCNT networks with tunable conductivity and transparency by a dry transfer technique, Nano Lett. 10 (2010) 4349–4355. https://doi.org/10.1021/nl101680s.

[60] A.G. Nasibulin, A. Kaskela, K. Mustonen, A.S. Anisimov, V. Ruiz, S. Kivistö, S. Rackauskas, M.Y. Timmermans, M. Pudas, B. Aitchison, M. Kauppinen, D.P. Brown, O.G. Okhotnikov, E.I. Kauppinen, Multifunctional free-standing single-walled carbon nanotube films, ACS Nano. 5 (2011) 3214–3221. https://doi.org/10.1021/nn200338r.

[61] J.A. Ramirez B., D.V. Krasnikov, V. V. Gubarev, I.V. Novikov, V.A. Kondrashov, A. V. Starkov, M.S. Krivokorytov, V.V. Medvedev, Y.G. Gladush, A.G. Nasibulin, Renewable single-walled carbon nanotube membranes for extreme ultraviolet pellicle applications, Carbon N Y. 198 (2022) 364–370. https://doi.org/10.1016/j.carbon.2022.07.014.

[62] A. Moisala, A.G. Nasibulin, D.P. Brown, H. Jiang, L. Khriachtchev, E.I. Kauppinen, Single-walled carbon nanotube synthesis using ferrocene and iron pentacarbonyl in a laminar flow reactor, Chem Eng Sci. 61 (2006) 4393–4402. https://doi.org/10.1016/j.ces.2006.02.020.

[63] A.G. Nasibulin, D.P. Brown, P. Queipo, D. Gonzalez, H. Jiang, E.I. Kauppinen, An essential role of CO_2 and H_2O during single-walled CNT synthesis from carbon monoxide, Chem Phys Lett. 417 (2006) 179–184. https://doi.org/10.1016/j.cplett.2005.10.022.

[64] D.V. Krasnikov, B.Y. Zabelich, V.Y. Iakovlev, A.P. Tsapenko, S.A. Romanov, A.A. Alekseeva, A.K. Grebenko, A.G. Nasibulin, A spark discharge generator for scalable aerosol CVD synthesis of single-walled carbon nanotubes with tailored

characteristics, Chemical Engineering Journal. 372 (2019) 462–470. https://doi.org/10.1016/j.cej.2019.04.173.

[65] V.Y. Iakovlev, D.V. Krasnikov, E.M. Khabushev, A.A. Alekseeva, A.K. Grebenko, A.P. Tsapenko, B.Y. Zabelich, J.V. Kolodiazhnaia, A.G. Nasibulin, Fine-tuning of spark-discharge aerosol CVD reactor for single-walled carbon nanotube growth: The role of ex situ nucleation, Chemical Engineering Journal. 383 (2020). https://doi.org/10.1016/j.cej.2019.123073.

[66] Y. Tian, M.Y. Timmermans, M. Partanen, A.G. Nasibulin, H. Jiang, Z. Zhu, E.I. Kauppinen, Growth of single-walled carbon nanotubes with controlled diameters and lengths by an aerosol method, Carbon. 49 (2011) 4636–4643. https://doi.org/10.1016/j.carbon.2011.06.036.

[67] Y. Tian, A.G. Nasibulin, B. Aitchison, T. Nikitin, J. V. Pfaler, H. Jiang, Z. Zhu, L. Khriachtchev, D.P. Brown, E.I. Kauppinen, Controlled synthesis of single-walled carbon nanotubes in an aerosol reactor, Journal of Physical Chemistry C. 115 (2011) 7309–7318. https://doi.org/10.1021/jp112291f.

[68] E.M. Khabushev, J.V. Kolodiazhnaia, D.V. Krasnikov, A.G. Nasibulin, Activation of catalyst particles for single-walled carbon nanotube synthesis, Chemical Engineering Journal. 413 (2021) 127475. https://doi.org/10.1016/j.cej.2020.127475.

[69] I. V. Anoshkin, A.G. Nasibulin, Y. Tian, B. Liu, H. Jiang, E.I. Kauppinen, Hybrid carbon source for single-walled carbon nanotube synthesis by aerosol CVD method, Carbon. 78 (2014) 130–136. https://doi.org/10.1016/j.carbon.2014.06.057.

[70] A.R. Bogdanova, D.V. Krasnikov, E.M. Khabushev, J.A. Ramirez B., Y.E. Matyushkin, A.G. Nasibulin, Role of Hydrogen in Ethylene-Based Synthesis of Single-Walled Carbon Nanotubes, Nanomaterials. 13 (2023) 1504. https://doi.org/10.3390/nano13091504.

[71] E.X. Ding, H. Jiang, Q. Zhang, Y. Tian, P. Laiho, A. Hussain, Y. Liao, N. Wei, E.I. Kauppinen, Highly conductive and transparent single-walled carbon nanotube thin films from ethanol by floating catalyst chemical vapor deposition, Nanoscale. 9 (2017) 17601–17609. https://doi.org/10.1039/c7nr05554d.

[72] E.X. Ding, A. Hussain, S. Ahmad, Q. Zhang, Y. Liao, H. Jiang, E.I. Kauppinen, High-performance transparent conducting films of long single-walled carbon nanotubes synthesized from toluene alone, Nano Res. 13 (2020) 112–120. https://doi.org/10.1007/s12274-019-2581-7.

[73] E.M. Khabushev, D.V. Krasnikov, A.E. Goldt, E.O. Fedorovskaya, A.P. Tsapenko, Q. Zhang, E.I. Kauppinen, T. Kallio, A.G. Nasibulin, Joint effect of ethylene and toluene on carbon nanotube growth, Carbon. 189 (2022) 474–483. https://doi.org/10.1016/j.carbon.2021.12.052.

[74] G. Glockler, Carbon-Oxygen Bond Energies and Bond Distances, The Journal of Physical Chemistry. 62 (1958) 1049-1054. https://pubs.acs.org/sharingguidelines.

[75]   K. Mustonen, P. Laiho, A. Kaskela, Z. Zhu, O. Reynaud, N. Houbenov, Y. Tian, T. Susi, H. Jiang, A.G. Nasibulin, E.I. Kauppinen, Gas phase synthesis of non-bundled, small diameter single-walled carbon nanotubes with near-armchair chiralities, Appl Phys Lett. 107 (2015). https://doi.org/10.1063/1.4926415.

[76]   Y. Liao, A. Hussain, P. Laiho, Q. Zhang, Y. Tian, N. Wei, E.X. Ding, S.A. Khan, N.N. Nguyen, S. Ahmad, E.I. Kauppinen, Tuning Geometry of SWCNTs by CO2 in Floating Catalyst CVD for High-Performance Transparent Conductive Films, Adv Mater Interfaces. 5 (2018). https://doi.org/10.1002/admi.201801209.

[77]   Y. Tian, M.Y. Timmermans, S. Kivistö, A.G. Nasibulin, Z. Zhu, H. Jiang, O.G. Okhotnikov, E.I. Kauppinen, Tailoring the diameter of single-walled carbon nanotubes for optical applications, Nano Res. 4 (2011) 807–815. https://doi.org/10.1007/s12274-011-0137-6.

[78]   A.G. Nasibulin, P. Queipo, S.D. Shandakov, D.P. Brown, H. Jiang, P. V. Pikhitsa, O. V. Tolochko, E.I. Kauppinen, Studies on mechanism of single-walled carbon nanotube formation, J Nanosci Nanotechnol. 6 (2006) 1233–1246. https://doi.org/10.1166/jnn.2006.340.

[79]   M.B. Bryning, D.E. Milkie, M.F. Islam, L.A. Hough, J.M. Kikkawa, A.G. Yodh, Carbon nanotube aerogels, Advanced Materials. 19 (2007) 661–664. https://doi.org/10.1002/adma.200601748.

[80]   X. Gui, J. Wei, K. Wang, A. Cao, H. Zhu, Y. Jia, Q. Shu, D. Wu, Carbon nanotube sponges, Advanced Materials. 22 (2010) 617–621. https://doi.org/10.1002/adma.200902986.

[81]   H. Sun, Z. Xu, C. Gao, Multifunctional, ultra-flyweight, synergistically assembled carbon aerogels, Advanced Materials. 25 (2013) 2554–2560. https://doi.org/10.1002/adma.201204576.

[82]   F. Schütt, S. Signetti, H. Krüger, S. Röder, D. Smazna, S. Kaps, S.N. Gorb, Y.K. Mishra, N.M. Pugno, R. Adelung, Hierarchical self-entangled carbon nanotube tube networks, Nat Commun. 8 (2017). https://doi.org/10.1038/s41467-017-01324-7.

[83]   SWCNT markets with the greatest potential, (n.d.) 10–12. DataM Intelligence, Global Carbon Nanotubes Market. https://www.datamintelligence.com/research-report/carbon-nanotubesmarket, 2023.

[84]   B. Arash, Q. Wang, V.K. Varadan, Mechanical properties of carbon nanotube/polymer composites, Sci Rep. 4 (2014) 1–8. https://doi.org/10.1038/srep06479.

[85]   M.T. Byrne, Y.K. Guin'Ko, Recent advances in research on carbon nanotube -polymer composites, Advanced Materials. 22 (2010) 1672–1688. https://doi.org/10.1002/adma.200901545.

[86] P.M. Ajayan, O. Stephan, C. Colliex, D. Trauth, Aligned Carbon Nanotube Arrays Formed by Cutting a Polymer Resin Aligned Carbon Nanotube Arrays Formed by Cutting a Polymer Resin Nanotube Composite Aligned Carbon Nanotube Arrays Formed by Cutting a Polymer Resin N …, 265 (2006) 11–12. https://doi.org/10.1126/science.265.5176.1212.

[87] W. Bauhofer, J.Z. Kovacs, T. Swan, T. Swan, T. Swan, A review and analysis of electrical percolation in carbon nanotube polymer composites, Compos Sci Technol. 69 (2009) 1486–1498. https://doi.org/10.1016/j.compscitech.2008.06.018.

[88] I. Balberg, C.H. Anderson, S. Alexander, N. Wagner, Excluded volume and its relation to the onset of percolation, Phys Rev B. 30 (1984) 3933. https://doi.org/10.1103/PhysRevB.30.3933

[89] A. Celzard, E. McRae, C. Deleuze, M. Dufort, Critical concentration in percolating systems containing a high-aspect-ratio filler, Phys Rev B Condens Matter Mater Phys. 53 (1996) 6209–6214. https://doi.org/10.1103/PhysRevB.53.6209.

[90] J.K.W. Sandler, J.E. Kirk, I.A. Kinloch, M.S.P. Shaffer, A.H. Windle, Ultra-low electrical percolation threshold in carbon-nanotube-epoxy composites, Polymer. 44 (2003) 5893–5899. https://doi.org/10.1016/S0032-3861(03)00539-1.

[91] A. Moisala, Q. Li, I.A. Kinloch, A.H. Windle, Thermal and electrical conductivity of single- and multi-walled carbon nanotube-epoxy composites, Compos Sci Technol. 66 (2006) 1285–1288. https://doi.org/10.1016/j.compscitech.2005.10.016.

[92] J.Z. Kovacs, B.S. Velagala, K. Schulte, W. Bauhofer, Two percolation thresholds in carbon nanotube epoxy composites, Composites Science and Technology. 67 (2007) 922–928. https://doi.org/10.1016/j.compscitech.2006.02.037.

[93] N.M. Nurazzi, M.R.M. Asyraf, A. Khalina, N. Abdullah, F.A. Sabaruddin, S.H. Kamarudin, S. Ahmad, A.M. Mahat, C.L. Lee, H.A. Aisyah, M.N.F. Norrrahim, R.A. Ilyas, M.M. Harussani, M.R. Ishak, S.M. Sapuan, Fabrication, functionalization, and application of carbon nanotube-reinforced polymer composite: An overview, Polymers (Basel). 13 (2021) 1–44. https://doi.org/10.3390/polym13071047.

[94] S. Gong, W. Cheng, One-Dimensional Nanomaterials for Soft Electronics, Adv Electron Mater. 3 (2017). https://doi.org/10.1002/aelm.201600314.

[95] S.H. Chae, Y.H. Lee, Carbon nanotubes and graphene towards soft electronics, Nano Converg. 1 (2014). https://doi.org/10.1186/s40580-014-0015-5.

[96] Y. Kato, M. Horibe, S. Ata, T. Yamada, K. Hata, Stretchable electromagnetic-interference shielding materials made of a long single-walled carbon-nanotube-elastomer composite, RSC Adv. 7 (2017) 10841–10847. https://doi.org/10.1039/c6ra25350d.

[97] B. Yao, W. Hong, T. Chen, Z. Han, X. Xu, R. Hu, J. Hao, C. Li, H. Li, S.E. Perini, M.T. Lanagan, S. Zhang, Q. Wang, H. Wang, Highly Stretchable Polymer Composite with Strain-Enhanced Electromagnetic Interference Shielding Effectiveness, Advanced Materials. 32 (2020) 1–7. https://doi.org/10.1002/adma.201907499.

[98] B. Shin, S. Mondal, M. Lee, S. Kim, Y. Il Huh, C. Nah, Flexible thermoplastic polyurethane-carbon nanotube composites for electromagnetic interference shielding and thermal management, Chemical Engineering Journal. 418 (2021) 129282. https://doi.org/10.1016/j.cej.2021.129282.

[99] W.L. Chan, J. Deibel, D.M. Mittleman, Imaging with terahertz radiation, Reports on Progress in Physics. 70 (2007) 1325–1379. https://doi.org/10.1088/0034-4885/70/8/R02.

[100] H.A. Hafez, X. Chai, A. Ibrahim, S. Mondal, D. Férachou, X. Ropagnol, T. Ozaki, Intense terahertz radiation and their applications, Journal of Optics (United Kingdom). 18 (2016). https://doi.org/10.1088/2040-8978/18/9/093004.

[101] J.H. Son, S.J. Oh, H. Cheon, Potential clinical applications of terahertz radiation, J Appl Phys. 125 (2019). https://doi.org/10.1063/1.5080205.

[102] J. Macutkevic, D. Seliuta, G. Valusis, R. Adomavicius, P. Kuzhir, A. Paddubskaya, M. Shuba, S. Maksimenko, L. Coderoni, F. Micciulla, I. Sacco, S. Bellucci, Terahertz time domain spectroscopy of epoxy resin composite with various carbon inclusions, Chem Phys. 404 (2012) 129–135. https://doi.org/10.1016/j.chemphys.2012.02.002.

[103] J. Macutkevic, D. Seliuta, G. Valusis, R. Adomavicius, A. Krotkus, P. Kuzhir, A. Paddubskaya, S. Maksimenko, V. Kuznetsov, I. Mazov, I. Simonova, Multi-walled carbon nanotubes/PMMA composites for THz applications, Diam Relat Mater. 25 (2012) 13–18. https://doi.org/10.1016/j.diamond.2012.02.002.

[104] D. Polley, A. Barman, R.K. Mitra, EMI shielding and conductivity of carbon nanotube- polymer composites at terahertz frequency, 39 (2014) 1541–1544.

[105] H.A. Butt, S. V Lomov, I.S. Akhatov, S.G. Abaimov, Self-diagnostic carbon nanocomposites manufactured from industrial epoxy masterbatches, Compos Struct. (2020) 113244. https://doi.org/10.1016/j.compstruct.2020.113244.

[106] V. Schroeder, S. Savagatrup, M. He, S. Lin, T.M. Swager, Carbon nanotube chemical sensors, Chem Rev. 119 (2019) 599–663. https://doi.org/10.1021/acs.chemrev.8b00340.

[107] W. Huang, K. Dai, Y. Zhai, H. Liu, P. Zhan, J. Gao, G. Zheng, C. Liu, C. Shen, Flexible and Lightweight Pressure Sensor Based on Carbon Nanotube/Thermoplastic Polyurethane-Aligned Conductive Foam with Superior Compressibility and Stability, ACS Appl Mater Interfaces. 9 (2017) 42266–42277. https://doi.org/10.1021/acsami.7b16975.

[108] M. Ji, H. Deng, D. Yan, X. Li, L. Duan, Q. Fu, Selective localization of multi-walled carbon nanotubes in thermoplastic elastomer blends: An effective method for tunable resistivity-strain sensing behavior, Compos Sci Technol. 92 (2014) 16–26. https://doi.org/10.1016/j.compscitech.2013.11.018.

[109] H. Liu, J. Gao, W. Huang, K. Dai, G. Zheng, C. Liu, C. Shen, X. Yan, J. Guo, Z. Guo, Electrically conductive strain sensing polyurethane nanocomposites with synergistic carbon nanotubes and graphene bifillers, Nanoscale. 8 (2016) 12977–12989. https://doi.org/10.1039/c6nr02216b.

[110] J.F. Christ, N. Aliheidari, A. Ameli, P. Pötschke, 3D printed highly elastic strain sensors of multiwalled carbon nanotube/thermoplastic polyurethane nanocomposites, Mater Des. 131 (2017) 394–401. https://doi.org/10.1016/j.matdes.2017.06.011.

[111] J.R. Bautista-Quijano, F. Avilés, J. V. Cauich-Rodriguez, Sensing of large strain using multiwall carbon nanotube/segmented polyurethane composites, J Appl Polym Sci. 130 (2013) 375–382. https://doi.org/10.1002/app.39177.

[112] T. Yamada, Y. Hayamizu, Y. Yamamoto, Y. Yomogida, A. Izadi-Najafabadi, D.N. Futaba, K. Hata, A stretchable carbon nanotube strain sensor for human-motion detection, Nat Nanotechnol. 6 (2011) 296–301. https://doi.org/10.1038/nnano.2011.36.

[113] K. Suzuki, K. Yataka, Y. Okumiya, S. Sakakibara, K. Sako, H. Mimura, Y. Inoue, Rapid-Response, Widely Stretchable Sensor of Aligned MWCNT/Elastomer Composites for Human Motion Detection, ACS Sens. 1 (2016) 817–825. https://doi.org/10.1021/acssensors.6b00145.

[114] I. Kang, M.J. Schulz, J.H. Kim, V. Shanov, D. Shi, A carbon nanotube strain sensor for structural health monitoring, Smart Mater Struct. 15 (2006) 737–748. https://doi.org/10.1088/0964-1726/15/3/009.

[115] H. Zhang, E. Bilotti, T. Peijs, The use of carbon nanotubes for damage sensing and structural health monitoring in laminated composites: a review, Nanocomposites. 1 (2015) 167–184. https://doi.org/10.1080/20550324.2015.1113639.

[116] G. Mittal, V. Dhand, K.Y. Rhee, S.J. Park, W.R. Lee, A review on carbon nanotubes and graphene as fillers in reinforced polymer nanocomposites, Journal of Industrial and Engineering Chemistry. 21 (2015) 11–25. https://doi.org/10.1016/j.jiec.2014.03.022.

[117] Z. Spitalsky, D. Tasis, K. Papagelis, C. Galiotis, Progress in Polymer Science Carbon nanotube – polymer composites : Chemistry , processing , mechanical and electrical properties, Prog Polym Sci. 35 (2010) 357–401. https://doi.org/10.1016/j.progpolymsci.2009.09.003.

[118] M.A. Kazakova, V.L. Kuznetsov, N. V. Semikolenova, S.I. Moseenkov, D. V. Krasnikov, M.A. Matsko, A. V. Ishchenko, V.A. Zakharov, A.I. Romanenko, O.B. Anikeeva, E.N. Tkachev, V.I. Suslyaev, V.A. Zhuravlev, K. V. Dorozkin,

Comparative study of multiwalled carbon nanotube/polyethylene composites produced via different techniques, Phys Status Solidi B Basic Res. 251 (2014) 2437–2443. https://doi.org/10.1002/pssb.201451194.

[119] P. Pötschke, B. Krause, S.T. Buschhorn, U. Köpke, M.T. Müller, T. Villmow, K. Schulte, Improvement of carbon nanotube dispersion in thermoplastic composites using a three roll mill at elevated temperatures, Compos Sci Technol. 74 (2013) 78–84. https://doi.org/10.1016/j.compscitech.2012.10.010.

[120] F. Du, J.E. Fischer, K.I. Winey, Coagulation Method for Preparing Single-Walled Carbon Nanotube / Poly (methyl methacrylate) Composites and Their Modulus , Electrical Conductivity , and Thermal Stability, (2003) 3333–3338.

[121] Y. Zheng, Y. Li, K. Dai, M. Liu, K. Zhou, G. Zheng, C. Liu, C. Shen, Conductive thermoplastic polyurethane composites with tunable piezoresistivity by modulating the filler dimensionality for flexible strain sensors, Compos Part A Appl Sci Manuf. 101 (2017) 41–49. https://doi.org/10.1016/j.compositesa.2017.06.003.

[122] B. Mensah, H.G. Kim, J.H. Lee, S. Arepalli, C. Nah, Carbon nanotube-reinforced elastomeric nanocomposites: A review, Int J Smart Nano Mater. 6 (2015) 211–238. https://doi.org/10.1080/19475411.2015.1121632.

[123] R. Sattar, A. Kausar, M. Siddiq, Advances in thermoplastic polyurethane composites reinforced with carbon nanotubes and carbon nanofibers: A review, Journal of Plastic Film and Sheeting. 31 (2015) 186–224. https://doi.org/10.1177/8756087914535126.

[124] Z. Sang, K. Ke, I. Manas-Zloczower, Effect of carbon nanotube morphology on properties in thermoplastic elastomer composites for strain sensors, Compos Part A Appl Sci Manuf. 121 (2019) 207–212. https://doi.org/10.1016/j.compositesa.2019.03.007.

[125] M. Dong, C. Wang, H. Liu, C. Liu, C. Shen, J. Zhang, C. Jia, T. Ding, Z. Guo, Enhanced Solid Particle Erosion Properties of Thermoplastic Polyurethane-Carbon Nanotube Nanocomposites, Macromol Mater Eng. 304 (2019) 1–11. https://doi.org/10.1002/mame.201900010.

[126] J.H. Du, J. Bai, H.M. Cheng, The present status and key problems of carbon nanotube based polymer composites, Express Polym Lett. 1 (2007) 253–273. https://doi.org/10.3144/expresspolymlett.2007.39.

[127] OCSiAl, Single-walled carbon nanotubes: structure, properties, applications, and health & safety. https://tuball.com/ru/articles/single-walled-carbon-nanotubes. 2023

[128] T.B. Nguyen Thi, S. Ata, T. Morimoto, T. Yamada, T. Okazaki, K. Hata, Tailoring the electrically conductive network of injection-molded polymer-carbon nanotube composite at low filler content, Mater Today Proc. 40 (2020) 5–8. https://doi.org/10.1016/j.matpr.2020.02.137.

[129] B.J.A. Gutierrez, S. Dul, A. Pegoretti, J. Alvarez-Quintana, L. Fambri, Investigation of the Effects of Multi-Wall and Single-Wall Carbon Nanotubes Concentration on the Properties of ABS Nanocomposites, C. 7 (2021) 33. https://doi.org/10.3390/c7020033.

[130] P. Pötschke, A.R. Bhattacharyya, A. Janke, S. Pegel, A. Leonhardt, C. Täschner, M. Ritschel, S. Roth, B. Hornbostel, J. Cech, Melt mixing as method to disperse carbon nanotubes into thermoplastic polymers, Fullerenes Nanotubes and Carbon Nanostructures. 13 (2005) 211–224. https://doi.org/10.1081/FST-200039267.

[131] K. Prashantha, J. Soulestin, M.F. Lacrampe, P. Krawczak, G. Dupin, M. Claes, Masterbatch-based multi-walled carbon nanotube filled polypropylene nanocomposites: Assessment of rheological and mechanical properties, Compos Sci Technol. 69 (2009) 1756–1763. https://doi.org/10.1016/j.compscitech.2008.10.005.

[132] OCSiAl, Technical data sheet. https://tuball.com/media/documents/files/2021/06/07/TDS_TUBALL_01RW03_ENG_V5.PDF. 2023.

[133] P.M. Kalachikova, A.E. Goldt, E.M. Khabushev, T. V. Eremin, K.B. Ustinovich, A. Grebenko, O.O. Parenago, T.S. Zatsepin, O.I. Pokrovskiy, E.D. Obraztsova, A.G. Nasibulin, Direct injection of SWCNTs into liquid after supercritical nitrogen treatment, Carbon. 152 (2019) 66–69. https://doi.org/10.1016/j.carbon.2019.06.003.

[134] K.B. Ustinovich, V. V. Ivanov, Y.M. Tokunov, A.A. Loshkarev, N.I. Sapronova, A.M. Vorobei, O.O. Parenago, M.G. Kiselev, Study of dispersions of carbon nanotubes modified by the method of rapid expansion of supercritical suspensions, Molecules. 25 (2020). https://doi.org/10.3390/molecules25184061.

[135] X. Liu, T. Pichler, T. Pichler, M. Knupfer, M.S. Golden, J. Fink, H. Kataura, Y. Achiba, Detailed analysis of the mean diameter and diameter distribution of single-wall carbon nanotubes from their optical response, Phys Rev B Condens Matter Mater Phys. 66 (2002) 454111–454118. https://doi.org/10.1103/PhysRevB.66.045411.

[136] K. Lingam, R. Podila, C. Loebick, P. Chen, P.C. Ke, B. Powell, L. Pfefferle, A.M. Rao, Effect of bundling on the π plasmon energy in sub-nanometer single wall carbon nanotubes, Carbon. 49 (2011) 3803–3807. https://doi.org/10.1016/j.carbon.2011.04.072.

[137] M. He, S. Zhang, J. Zhang, Horizontal Single-Walled Carbon Nanotube Arrays: Controlled Synthesis, Characterizations, and Applications, Chem Rev. 120 (2020) 12592–12684. https://doi.org/10.1021/acs.chemrev.0c00395.

[138] S.A. Romanov, A.E. Aliev, B. V. Fine, A.S. Anisimov, A.G. Nasibulin, Highly efficient thermophones based on freestanding single-walled carbon nanotube films, Nanoscale Horiz. 4 (2019) 1158–1163. https://doi.org/10.1039/c9nh00164f.

[139] J.A. Creighton, D.G. Eadont, Ultraviolet-Visible Absorption Spectra of the Colloidal Metallic Elements, Journal pf the Chemical Society, Faraday Transactions. 87 (1991) 3881-3891. https://doi.org/10.1039/FT9918703881

[140] L. Guo, Q. Huang, X.Y. Li, S. Yang, Iron nanoparticles: Synthesis and applications in surface enhanced Raman scattering and electrocatalysis, Physical Chemistry Chemical Physics. 3 (2001) 1661–1665. https://doi.org/10.1039/b009951l.

[141] L. Calliari, S. Fanchenko, M. Filippi, Plasmon features in electron energy loss spectra from carbon materials, Carbon. 45 (2007) 1410–1418. https://doi.org/10.1016/j.carbon.2007.03.034.

[142] A. Jorio, M.A. Pimenta, A.G. Souza Filho, R. Saito, G. Dresselhaus, M.S. Dresselhaus, Characterizing carbon nanotube samples with resonance Raman scattering, New J Phys. 5 (2003). https://doi.org/10.1088/1367-2630/5/1/139.

[143] M.S. Dresselhaus, G. Dresselhaus, R. Saito, A. Jorio, Raman spectroscopy of carbon nanotubes, 409 (2005) 47–99. https://doi.org/10.1016/j.physrep.2004.10.006.

[144] A.S. Anisimov, A.G. Nasibulin, H. Jiang, P. Launois, J. Cambedouzou, S.D. Shandakov, E.I. Kauppinen, Mechanistic investigations of single-walled carbon nanotube synthesis by ferrocene vapor decomposition in carbon monoxide, Carbon N Y. 48 (2010) 380–388. https://doi.org/10.1016/j.carbon.2009.09.040.

[145] A. Kaskela, P. Laiho, N. Fukaya, K. Mustonen, T. Susi, H. Jiang, N. Houbenov, Y. Ohno, E.I. Kauppinen, Highly individual SWCNTs for high performance thin film electronics, Carbon. 103 (2016) 228–234. https://doi.org/10.1016/j.carbon.2016.02.099.

[146] A. Moisala, A.G. Nasibulin, I. Kauppinen, The role of metal nanoparticles in the catalytic production of single-walled carbon nanotubes-a review, Journal of Physics: Condensed Matter. 15 (2003) S3011. https://doi.org/10.1088/0953-8984/15/42/003

[147] A.G. Nasibulin, P.V. Pikhitsa, H. Jiang, E.I. Kauppinen, Correlation between catalyst particle and single-walled carbon nanotube diameters, Carbon. 43 (2005) 2251–2257. https://doi.org/10.1016/j.carbon.2005.03.048.

[148] M.C. Diaz, H. Jiang, E. Kauppinen, R. Sharma, P.B. Balbuena, Can Single-Walled Carbon Nanotube Diameter Be Defined by Catalyst Particle Diameter?, Journal of Physical Chemistry C. 123 (2019) 30305–30317. https://doi.org/10.1021/acs.jpcc.9b07724.

[149] P. Kulkarni, P.A. (Paul A. Baron, Klaus. Willeke, Aerosol measurement : principles, techniques, and applications, Wiley, 2011.

[150] D.R. Chen, M. Chitranshi, M. Schulz, V. Shanov, A Review of Three Major Factors Controlling Carbon Nanotubes Synthesis from the Floating Catalyst

Chemical Vapor Deposition, Nano Life. 09 (2019) 1930002.
https://doi.org/10.1142/s1793984419300024.

[151] A.R. Bogdanova, D. V. Krasnikov, A.G. Nasibulin, The role of sulfur in the CVD carbon nanotube synthesis, Carbon N Y. 210 (2023) 118051.
https://doi.org/10.1016/j.carbon.2023.118051.

[152] K. Mustonen, P. Laiho, A. Kaskela, T. Susi, A.G. Nasibulin, E.I. Kauppinen, Uncovering the ultimate performance of single-walled carbon nanotube films as transparent conductors, Appl Phys Lett. 107 (2015).
https://doi.org/10.1063/1.4932942.

[153] O. Reynaud, A.G. Nasibulin, A.S. Anisimov, I. V. Anoshkin, H. Jiang, E.I. Kauppinen, Aerosol feeding of catalyst precursor for CNT synthesis and highly conductive and transparent film fabrication, Chemical Engineering Journal. 255 (2014) 134–140. https://doi.org/10.1016/j.cej.2014.06.082.

[154] J.S. Bulmer, A. Kaniyoor, T. Gspann, J. Mizen, J. Ryley, P. Kiley, G. Ratering, W. Sparreboom, G. Bauhuis, T. Stehr, D. Oudejans, M. Sparkes, B. O'Neill, J.A. Elliott, Forecasting continuous carbon nanotube production in the floating catalyst environment, Chemical Engineering Journal. 390 (2020) 124497.
https://doi.org/10.1016/j.cej.2020.124497.

[155] Y. Ma, A.B. Dichiara, D. He, L. Zimmer, J. Bai, Control of product nature and morphology by adjusting the hydrogen content in a continuous chemical vapor deposition process for carbon nanotube synthesis, Carbon. 107 (2016) 171–179.
https://doi.org/10.1016/j.carbon.2016.05.060.

[156] J. Lei, K. V. Bets, E.S. Penev, B.I. Yakobson, Floating Fe Catalyst Formation and Effects of Hydrogen Environment in the Growth of Carbon Nanotubes, J Phys Chem Lett. 14 (2023) 4266–4272. https://doi.org/10.1021/acs.jpclett.3c00716.

[157] Q. Liu, W. Ren, Z.G. Chen, D.W. Wang, B. Liu, B. Yu, F. Li, H. Cong, H.M. Cheng, Diameter-selective growth of single-walled carbon nanotubes with high quality by floating catalyst method, ACS Nano. 2 (2008) 1722–1728.
https://doi.org/10.1021/nn8003394.

[158] P.X. Hou, W.S. Li, S.Y. Zhao, G.X. Li, C. Shi, C. Liu, H.M. Cheng, Preparation of metallic single-wall carbon nanotubes by selective etching, ACS Nano. 8 (2014) 7156–7162. https://doi.org/10.1021/nn502120k.

[159] A.R. Bogdanova, D. V Krasnikov, E.M. Khabushev, J.A. Ramirez, Y. Matyushkin, A.G. Nasibulin, Role of hydrogen in carbon nanotube synthesis, n.d.
https://ssrn.com/abstract=4305756.

[160] A.M. Shetty, G.M.H. Wilkins, J. Nanda, M.J. Solomon, Multiangle depolarized dynamic light scattering of short functionalized single-walled carbon nanotubes, Journal of Physical Chemistry C. 113 (2009) 7129–7133.
https://doi.org/10.1021/jp900731q.

[161] S. Badaire, P. Poulin, M. Maugey, C. Zakri, In situ measurements of nanotube dimensions in suspensions by depolarized dynamic light scattering, Langmuir. 20 (2004) 10367–10370. https://doi.org/10.1021/la049096r.

[162] D.E. Tsentalovich, A.W.K. Ma, J.A. Lee, N. Behabtu, E.A. Bengio, A. Choi, J. Hao, Y. Luo, R.J. Headrick, M.J. Green, Y. Talmon, M. Pasquali, Relationship of Extensional Viscosity and Liquid Crystalline Transition to Length Distribution in Carbon Nanotube Solutions, Macromolecules. 49 (2016) 681–689. https://doi.org/10.1021/acs.macromol.5b02054.

[163] P. Karlsen, M. V. Shuba, C. Beckerleg, D.I. Yuko, P.P. Kuzhir, S.A. Maksimenko, V. Ksenevich, H. Viet, A.G. Nasibulin, R. Tenne, E. Hendry, Influence of nanotube length and density on the plasmonic terahertz response of single-walled carbon nanotubes, J Phys D Appl Phys. 51 (2018). https://doi.org/10.1088/1361-6463/aa96ef.

[164] G. Chen, R.C. Davis, H. Kimura, S. Sakurai, M. Yumura, D.N. Futaba, K. Hata, The relationship between the growth rate and the lifetime in carbon nanotube synthesis, Nanoscale. 7 (2015) 8873–8878. https://doi.org/10.1039/c5nr01125f.

[165] C.T. Wirth, B.C. Bayer, A.D. Gamalski, S. Esconjauregui, R.S. Weatherup, C. Ducati, C. Baehtz, J. Robertson, S. Hofmann, The phase of iron catalyst nanoparticles during carbon nanotube growth, Chemistry of Materials. 24 (2012) 4633–4640. https://doi.org/10.1021/cm301402g.

[166] J.S. Bulmer, T.S. Gspann, J.S. Barnard, J.A. Elliott, Chirality-independent characteristic crystal length in carbon nanotube textiles measured by Raman spectroscopy, Carbon N Y. 115 (2017) 672–680. https://doi.org/10.1016/j.carbon.2017.01.044.

[167] J. Vaillancourt, H. Zhang, P. Vasinajindakaw, H. Xia, X. Lu, X. Han, D.C. Janzen, W.S. Shih, C.S. Jones, M. Stroder, M.Y. Chen, H. Subbaraman, R.T. Chen, U. Berger, M. Renn, All ink-jet-printed carbon nanotube thin-film transistor on a polyimide substrate with an ultrahigh operating frequency of over 5 GHz, Appl Phys Lett. 93 (2008). https://doi.org/10.1063/1.3043682.

[168] K. Kordás, T. Mustonen, G. Tóth, H. Jantunen, M. Lajunen, C. Soldano, S. Talapatra, S. Kar, R. Vajtai, P.M. Ajayan, Inkjet printing of electrically conductive patterns of carbon nanotubes, Small. 2 (2006) 1021–1025. https://doi.org/10.1002/smll.200600061.

[169] H. Okimoto, T. Takenobu, K. Yanagi, Y. Miyata, H. Shimotani, H. Kataura, Y. Iwasa, Tunable carbon nanotube thin-film transistors produced exclusively via inkjet printing, Advanced Materials. 22 (2010) 3981–3986. https://doi.org/10.1002/adma.201000889.

[170] R.D. Bennett, A.J. Hart, A.C. Miller, P.T. Hammond, D.J. Irvine, R.E. Cohen, Creating patterned carbon nanotube catalysts through the microcontact printing of

block copolymer micellar thin films, Langmuir. 22 (2006) 8273–8276. https://doi.org/10.1021/la061054a.

[171] K.N. Han, C.A. Li, M.P.N. Bui, G.H. Seong, Patterning of single-walled carbon nanotube films on flexible, transparent plastic substrates, Langmuir. 26 (2010) 598–602. https://doi.org/10.1021/la9021273.

[172] M.R.S. Castro, A.F. Lasagni, H.K. Schmidt, F. Mücklich, Direct laser interference patterning of multi-walled carbon nanotube-based transparent conductive coatings, Appl Surf Sci. 254 (2008) 5874–5878. https://doi.org/10.1016/j.apsusc.2008.03.140.

[173] C. Lim, D.H. Min, S.B. Lee, Direct patterning of carbon nanotube network devices by selective vacuum filtration, Appl Phys Lett. 91 (2007). https://doi.org/10.1063/1.2824575.

[174] L.D. Tijing, C.H. Park, W.L. Choi, M.T.G. Ruelo, A. Amarjargal, H.R. Pant, I.T. Im, C.S. Kim, Characterization and mechanical performance comparison of multiwalled carbon nanotube/polyurethane composites fabricated by electrospinning and solution casting, Compos B Eng. 44 (2013) 613–619. https://doi.org/10.1016/j.compositesb.2012.02.015.

[175] W. Chen, X. Tao, Y. Liu, Carbon nanotube-reinforced polyurethane composite fibers, Compos Sci Technol. 66 (2006) 3029–3034. https://doi.org/10.1016/j.compscitech.2006.01.024.

[176] B.E. Kilbride, J.N. Coleman, J. Fraysse, P. Fournet, Experimental observation of scaling laws for alternating current and direct current conductivity in polymer-carbon nanotube composite thin films, 4024 (2002). https://doi.org/10.1063/1.1506397.

[177] S. Geng, P. Wang, T. Ding, Impedance characteristics and electrical modelling of multi-walled carbon nanotube/silicone rubber composites, Compos Sci Technol. 72 (2011) 36–40. https://doi.org/10.1016/j.compscitech.2011.08.021.

[178] H. Xia, M. Song, Preparation and characterization of polyurethane-carbon nanotube composites, Soft Matter. 1 (2005) 386–394. https://doi.org/10.1039/b509038e.

[179] NIST Chemistry WebBook Database. https://webbook.nist.gov, 2023.

[180] A.T.D. Butland, R.J. Maddison, The specific heat of graphite: an evaluation of measurements, J Nucl Mater. 49 (1973/74) 45-56. https://doi.org/10.1016/0022-3115(73)90060-3.

Appendices

Appendix 1. Theoretical prerequisites for improvement of film equivalent sheet resistance by patterning (rational design).

Then let us consider patterned conductive film in a shape of square grid (**Figure 3a**). To highlight its advantages more, we discuss grid cut of the continuous TCF introduced in the previous paragraph. Therefore, the grid line transmittance is T_0 as well as its sheet resistance is R_0. We will use such a characteristic structural parameter of the grid as a filling factor f (equation (13)). Using this parameter, we can calculate the overall transmittance of the grid T:

$$T = (1 - f) \cdot 1 + f \cdot T_0 = 1 - f + fT_0. \tag{A1}$$

Next, we estimate overall resistance of the grid R taking into account the part "lost" at "cutting" continuous film to grid:

$$R = R_0 \frac{p}{w} = \frac{R_0}{1 - \sqrt{1 - f}}. \tag{A2}$$

Likewise it was defined for continuous film (equation (11)), equivalent resistance of the grid is calculated for 90% transmittance at 550 nm:

$$R_{90} = R \frac{\log T}{\log 0.9} = \frac{R_0}{1 - \sqrt{1 - f}} \cdot \frac{\log(1 - f + fT_0)}{\log 0.9}. \tag{A3}$$

Here, it is worth noting that 90% total transmittance for patterned film in principle cannot be reached at certain conditions, such as very low grid line transmittance T_0 and high filling factor. Therefore, R_{90} is rather mathematical description than physical phenomenon here.

Yet, definitely, the cases we are interested in suggest that 90% transmittance of the film is achievable in principle.

Finally, let us derive an expression for the R_{90}/R_{90}^0 ratio as a main indicator of the patterning efficiency:

$$\alpha \equiv \frac{R_{90}}{R_{90}^0} = \frac{1}{1 - \sqrt{1-f}} \cdot \frac{\log(1-f+fT_0)}{\log T_0}, \tag{A4}$$

where we denote the R_{90}/R_{90}^0 ratio as α.

Appendix 2. Bundling degree dependency on number of nanotubes and residence time

Bundle diameter, d_b, is connected to the bundling degree according to equation (33):

$$d_b = db^{\frac{1}{2}} = d\left(\frac{N}{N_b}\right)^{\frac{1}{2}}. \tag{A5}$$

Thus, coagulation K coefficient is dependent on time t and aerosol concentration $N(t)$ [149]:

$$K = \frac{4kTC_c}{3\mu} \sim C_c \sim Kn \sim \frac{\lambda_{mean\,free}}{d_m} \sim d_m^{-1} \sim L^{-\frac{1}{3}}d_b^{-\frac{2}{3}} \sim L^{-\frac{1}{3}}N(t)^{-\frac{1}{3}} \sim L^{-\frac{1}{3}}N(t)^{-\frac{1}{3}} \sim$$
$$\sim t^{-\frac{\lambda}{3}}N(t)^{-\frac{1}{3}} = \alpha t^{-\frac{\lambda}{3}}N(t)^{-\frac{1}{3}}, \tag{A6}$$

where C_c is the Cunningham slip correction factor, μ is gas viscosity, $\lambda_{mean\,free}$ is mean free path, and α is a proportionality coefficient. Thus, the following differential equation is derived:

$$\frac{dN(t)}{dt} = -\alpha t^{-\frac{\lambda}{3}}N(t)^{-\frac{1}{3}}N(t)^2 = -\alpha t^{-\frac{\lambda}{3}}N(t)^{\frac{5}{3}}. \tag{A7}$$

Having integrated this differential equation, we may derive the dependency of the bundling

degree on the number of formed SWCNTs and residence time (considering the following

initial conditions $N(0) = N; N(\tau) = N_b$):

$$N(t) = \frac{N(0)}{\left(1 + \frac{2\alpha}{3 - \lambda} \cdot N(0)^{\frac{2}{3}} \cdot t^{\frac{3-\lambda}{3}}\right)^{\frac{3}{2}}},$$

$$b = \frac{N}{N_b} = N \left/ \frac{N}{\left(1 + \frac{2\alpha}{3 - \lambda} \cdot N^{\frac{2}{3}} \cdot \tau^{\frac{3-\lambda}{3}}\right)^{\frac{3}{2}}} \right. = \left(1 + \frac{2\alpha}{3 - \lambda} \cdot N^{\frac{2}{3}} \cdot \tau^{\frac{3-\lambda}{3}}\right)^{\frac{3}{2}} \sim N \cdot \tau^{\frac{3-\lambda}{2}}. \quad (A8)$$

Appendix 3. Thermodynamic calculations for CO/H₂ atmosphere.

To estimate equilibrium concentrations of the products of reactions (18) – (19), the

correlation between change in Gibbs free energy $\Delta_r G^0$ and equilibrium constant K_{eq} was

used:

$$K_{eq} = \exp\left(-\frac{\Delta_r G^0}{RT}\right). \quad (A9)$$

Meanwhile, $\Delta_r G^0$ can be expressed as a difference between free energies of the product

$\Delta_f G_{product}$ and reactant $\Delta_f G_{reactant}$ formation:

$$\Delta_r G^0 = \Delta_f G_{product}(T) - \Delta_f G_{reactant}(T), \quad (A10)$$

where free energy of the reagent formation can be derived using the enthalpy $\Delta_f H$ and

entropy $\Delta_f S$ formation:

$$\Delta_f G(T) = \Delta_f H(T) - T\Delta_f S(T), \quad (A11)$$

146

which temperature dependency, in turn, can be derived using heat capacity C_p:

$$\Delta_f H(T) = \Delta_f H(298 \text{ K}) + \int_{298}^{T} C_p(T)dT, \tag{A12}$$

$$\Delta_f S(T) = \Delta_f S(298 \text{ K}) + \int_{298}^{T} \frac{C_p(T)}{T} dT, \tag{A13}$$

where $\Delta_f H(298 \text{ K})$ and $\Delta_f S(298 \text{ K})$ are standard enthalpy and entropy, respectively. Using polynomial heat capacity dependency on reduced temperature $\tau = \frac{T}{1000}$ (K) (Shomate equation):

$$C_p = A + B\tau + C\tau^2 + D\tau^3 + \frac{E}{\tau^2}, \tag{A15}$$

and using the equations (S4) and (S5) we can derive temperature-dependent $\Delta_f H(\tau)$ and $\Delta_f S(\tau)$:

$$\Delta_f H(\tau) = A\tau + \frac{B\tau^2}{2} + \frac{C\tau^3}{3} + \frac{D\tau^4}{4} - \frac{E}{\tau} + F, \tag{A16}$$

$$\Delta_f S(\tau) = A\ln\tau + B\tau + \frac{C\tau^2}{2} + \frac{D\tau^3}{3} - \frac{E}{2\tau^2} + G, \tag{A17}$$

where the coefficients used can be found in NIST database (**Table A1**, [179]). The resulting $\Delta_f G(T)$-vs-T curves for reactions (18) – (20) are plotted in **Figure 13a**.

Table A1. Coefficients from Shomate equation for the reagents from reactions (3) – (5) (taken from NIST database [179]; empirical coefficients for C (graphite) were taken from [180]).

Reagent	A	B	C	D	E	F	G

CO (<1300 K)	25.56759	6.09613	4.054656	-2.6713	0.131021	-118.009	227.3665
CO (>1300 K)	35.1507	1.300095	-0.20592	0.01355	-3.28278	-127.838	231.712
CO_2 (<1200 K)	24.99735	55.18696	-33.6914	7.948387	-0.13664	-403.608	228.2431
CO_2 (>1200 K)	58.16639	2.720074	-0.49229	0.038844	-6.44729	-425.919	263.6125
C (graphite)	0.538657	9.11E-06	-90.2725	-43449.3	1.59E07	-1.44E+09	5.74
H_2 (<1000 K)	33.06618	-11.3634	11.43282	-2.77287	-0.15856	-9.9808	172.708
H_2 (>1000 K)	18.56308	12.25736	-2.85979	0.268238	1.97799	-1.14744	156.2881
H_2O	30.092	6.832514	6.793435	-2.53448	0.082139	-250.881	223.3967
CH_4 (<1300 K)	-0.70303	108.4773	-42.5216	5.862788	0.678565	-76.8438	158.7163
CH_4 (>1300 K)	85.81217	11.26467	-2.11415	0.13819	-26.4222	-153.533	224.4143

The quotients of reactions (18) – (20) (Q_1, Q_2, Q_3) are calculated according to the equations:

$$Q_1 = \frac{\{CO_2\}}{\{CO\}^2}, \tag{A18}$$

$$Q_2 = \frac{\{H_2O\}}{\{CO\}\{H_2\}}, \tag{A19}$$

$$Q_3 = \frac{\{CH_4\}}{\{H_2\}^2}, \tag{A20}$$

where actual concentrations of the reagents are denoted as reagents in curly brackets. At the equilibrium, the quotients turn to equilibrium constants (K_1, K_2, K_3). Calculated

equilibrium constants allow determining equilibrium concentrations of the products of reactions (18) - (20) (denoted as reagents in square brackets): CO_2, H_2O, and CH_4 depending on the H_2 concentration:

$$K_1 = \frac{[CO_2]}{[CO]^2}, \tag{A21}$$

$$K_2 = \frac{[H_2O]}{[CO][H_2]}, \tag{A22}$$

$$K_3 = \frac{[CH_4]}{[H_2]^2}. \tag{A23}$$

Taking into account that the reactor is kept under atmospheric pressure and describing equilibrium concentration in vol%, total concentration of CO and H_2 equals to 1 (100 vol%). Thus, considering initial concentration of the introduced hydrogen as a parameter a ($[H_2] \equiv a$), CO concentration is determined by a ($[CO] \equiv 1 - a$), the products (their equilibrium concentrations) taken as sought variables (extents of reaction) ($[CO_2] \equiv x$, $[H_2O] \equiv y$, $[CH_4] \equiv z$), and taking into account consumption of the reagents (CO and H_2), we can obtain the system of equations:

$$\begin{cases} K_1 = \dfrac{x}{(1 - a - 2x - y)^2} \\ K_2 = \dfrac{y}{(1 - a - 2x - y)(a - y - 2z)} \\ K_3 = \dfrac{z}{(a - y - 2z)^2} \end{cases}, \tag{A24}$$

where equilibrium constants are known for the given temperature. The system of equations (A24) can be solved numerically for parameter a in the range of (0,1). **Figure A1** represents the results of equation (A24) solution for both temperatures: 880 °C and 1000 °C.
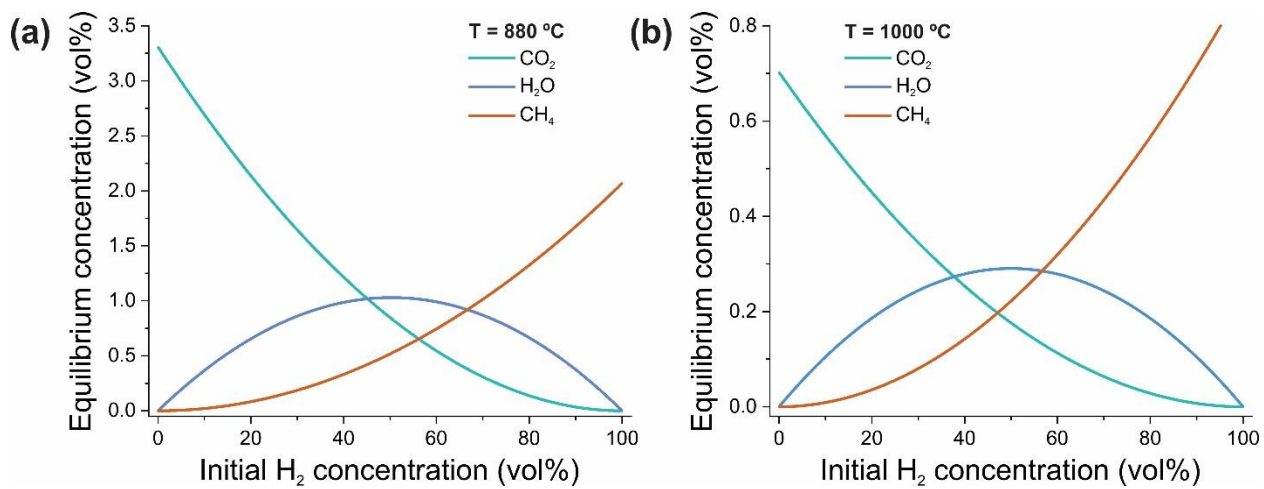
Figure S1. Calculated equilibrium concentrations of CO_2, H_2O, and CH_4 depending on the initial H_2 concentration introduced at **(a)** 880 °C and **(b)** 1000 °C.

Appendix 4. Effects of nitrogen and residence time in H₂-assisted aerosol CVD nanotube synthesis.
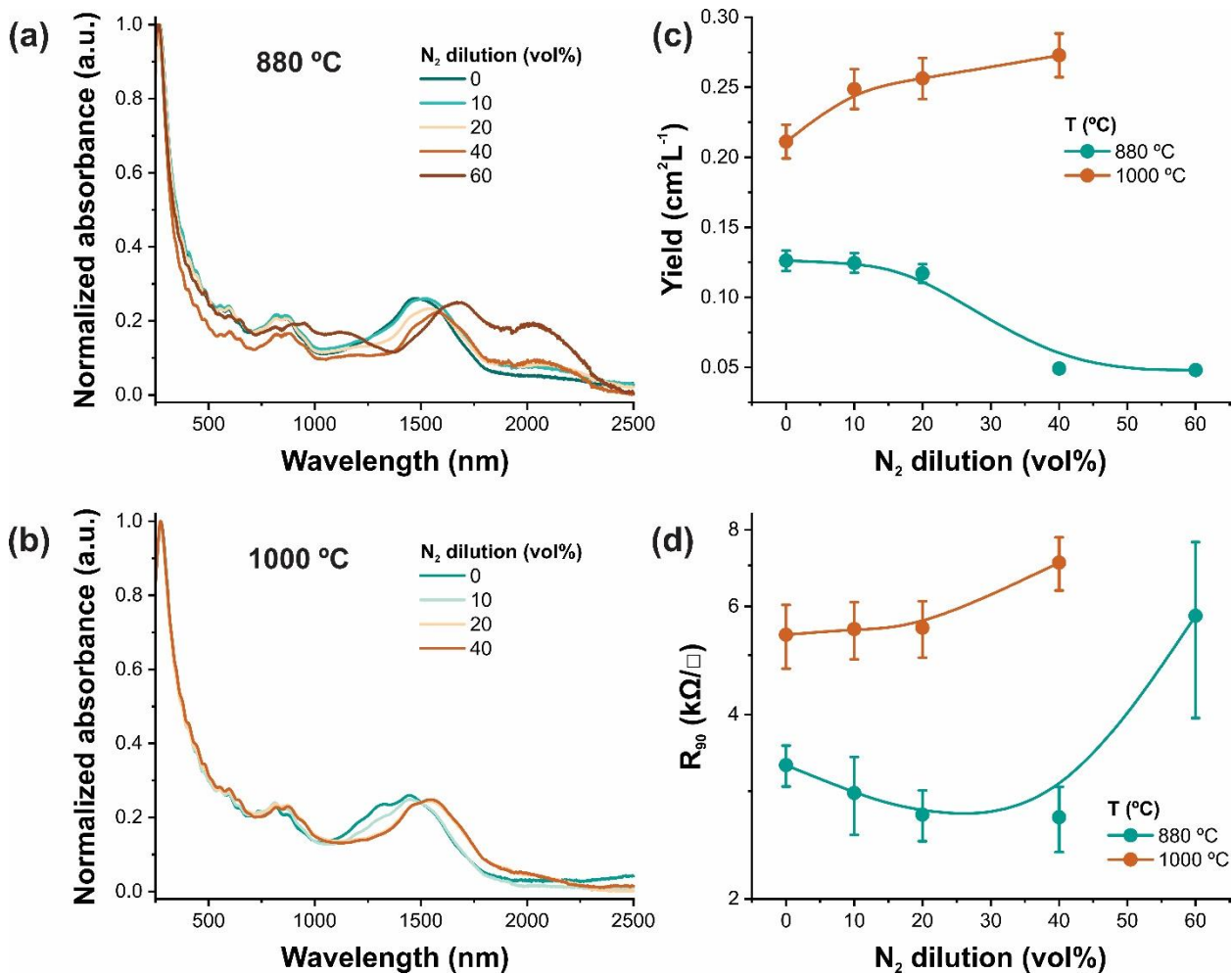
Figure A2. UV-vis-NIR spectra of the SWCNT films synthesized with N_2 dilution (concentration is shown in the legend) at **(a)** 880 °C and **(b)** 1000 °C; Dependencies of the yield **(c)** and R_{90} **(d)** on N_2 concentration at 880 °C and 1000 °C.
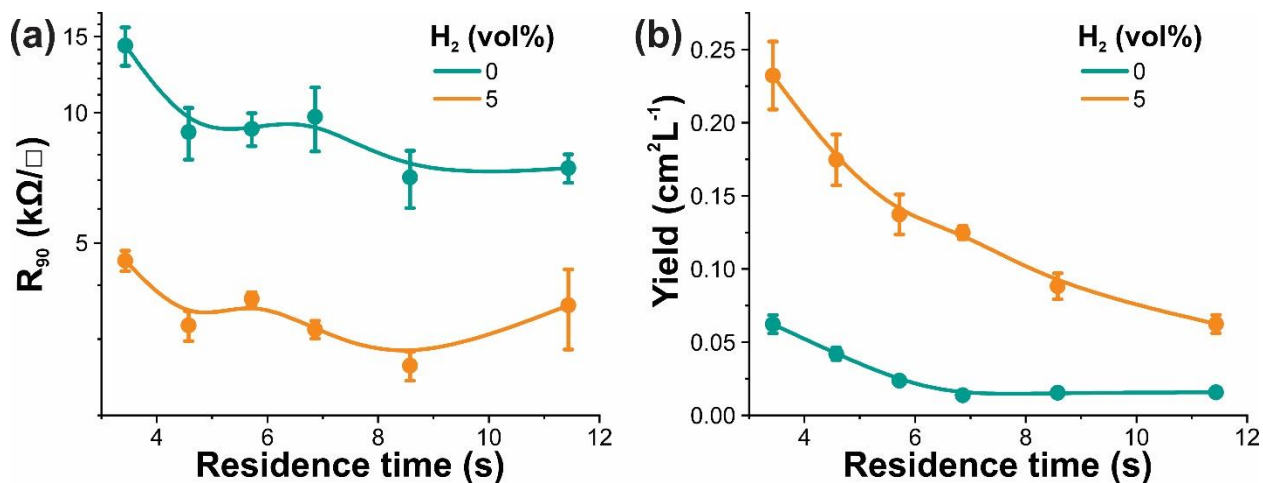
Figure A3. (a) R_{90} and **(b)** yield dependencies on residence time without and with H_2 introduction (at 5 vol%) at 1000 °C.

Appendix 5. Supporting figures for nanotube kinetics evaluation study
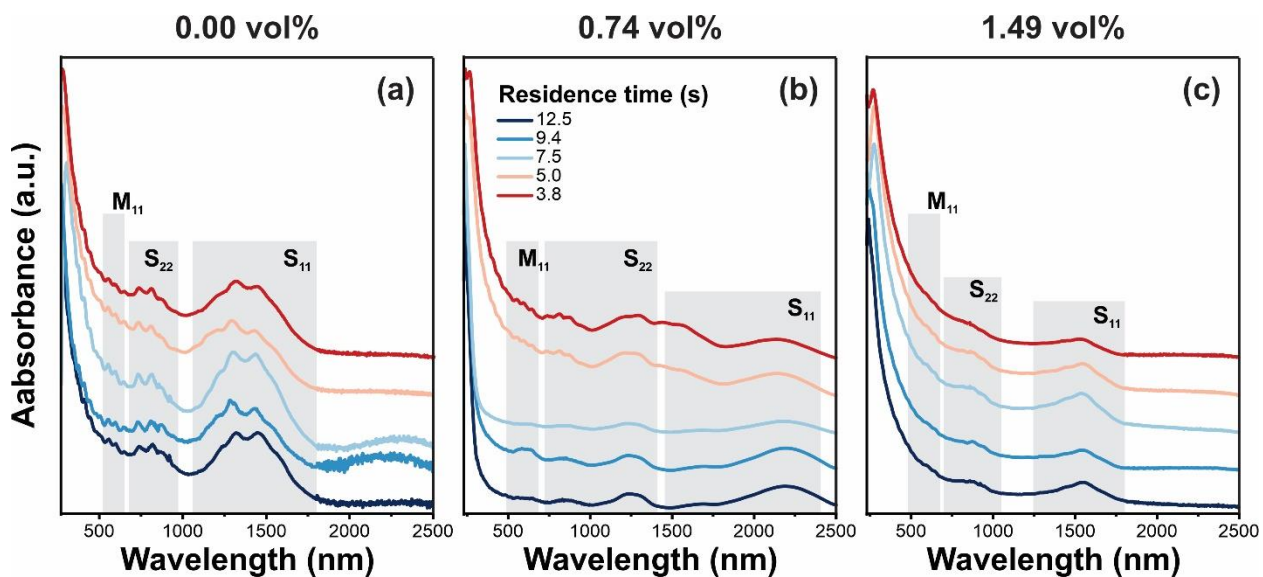
Figure A4. UV-vis-NIR (optical absorbance) spectra with highlighted transition peaks of SWCNTs synthesized at different residence times (shown in the legend) and CO_2 concentrations: (a) 0.00 vol%, (b) 0.74 vol%, (c) 1.49 vol%.
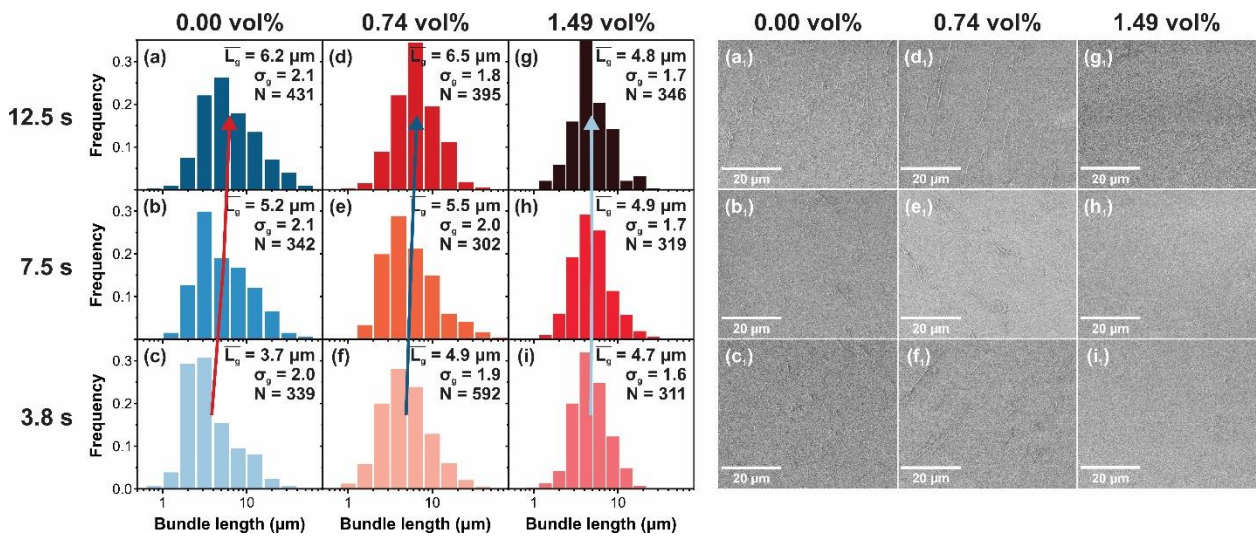
Figure A5. Bundle length distribution histograms of SWCNTs synthesized at different residence times (image rows) and CO_2 concentrations (image columns) indicated in figure: **(a)-(c)** 0.00 vol%, **(d)-(f)** 0.74 vol%, **(g)-(i)** 1.49 vol%. Arrows indicate a shift in geometric mean length with τ. **(a_1-i_1)** Corresponding typical SEM images of SWCNT bundles on Si/SiO$_2$ substrate.
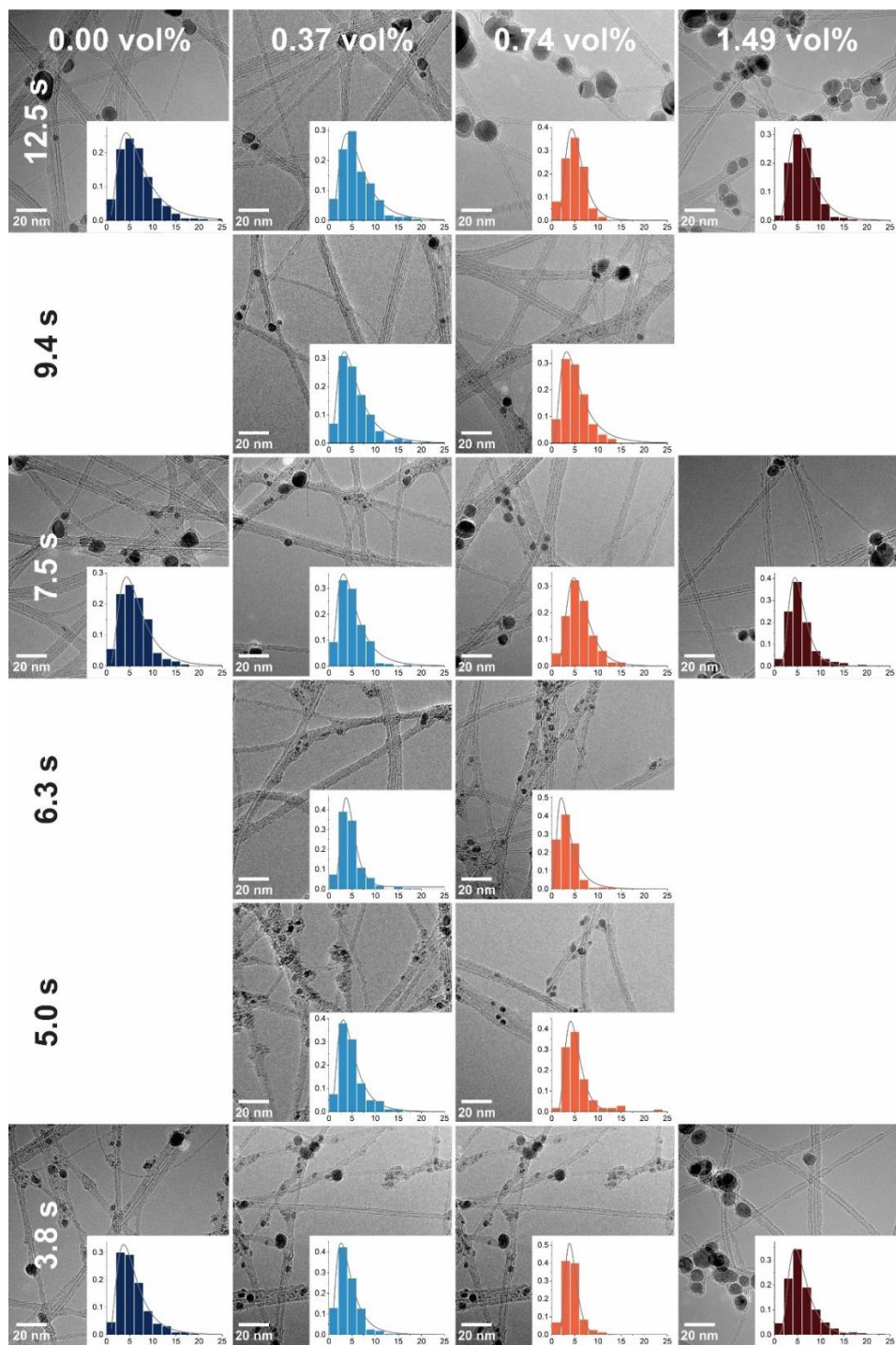
Figure A6. Typical TEM images of SWCNTs synthesized at different τ and $c(CO_2)$ (see indicated rows and columns, respectively) with corresponding bundle diameter distribution histograms.
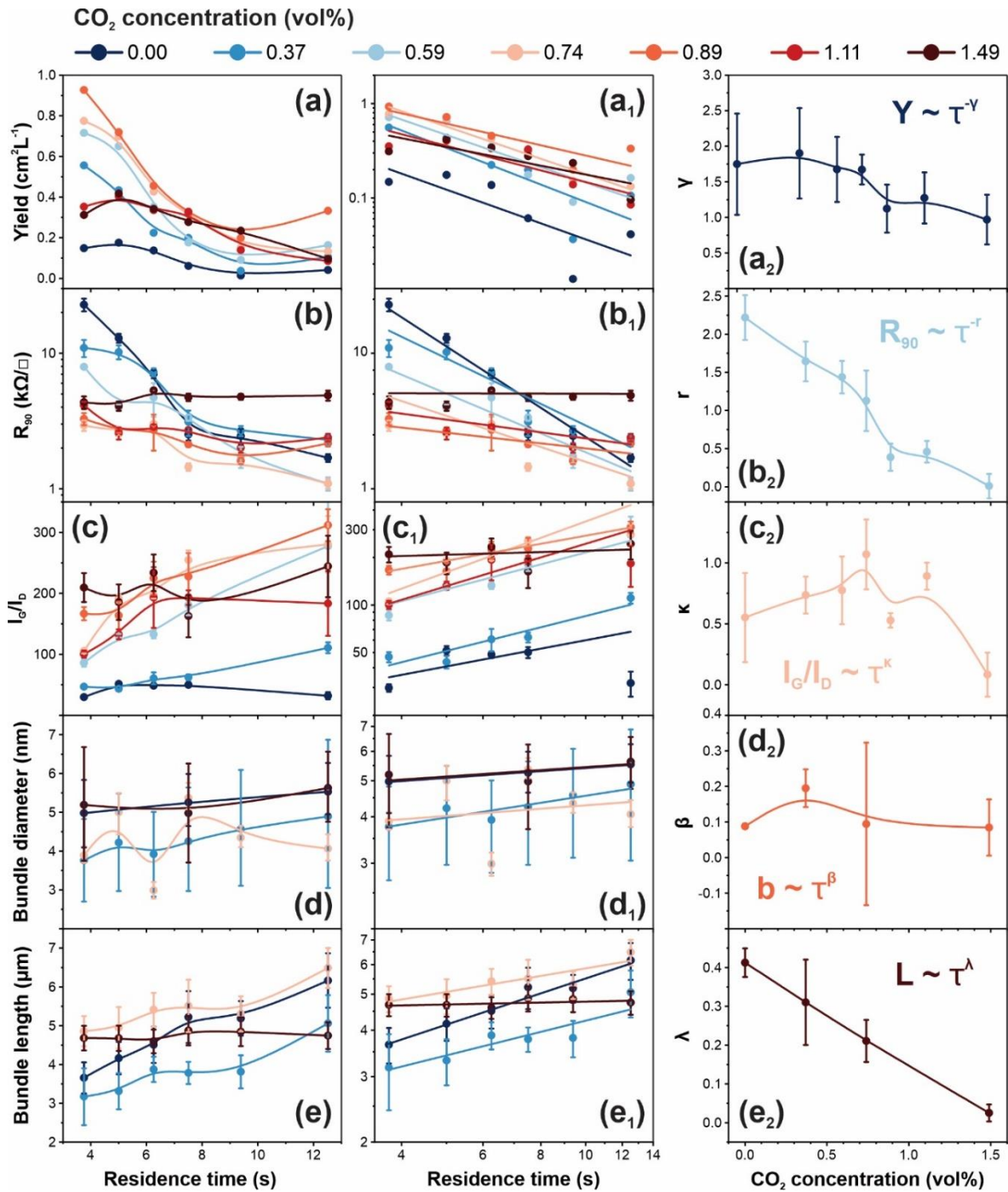
Figure A7. Dependencies of **(a)** yield, **(b)** R_{90}, **(c)** I_G/I_D, **(d)** bundle diameter, and **(e)** bundle length on residence time at different $c(CO_2)$ (shown in the legend at the top of the image); **(a₁-e₁)** the same dependencies plotted in log-log scales. Dependencies of exponents in scaling laws of **(a₂)** γ (Y-vs-τ), **(b₂)** r (σ_{90}-vs-τ), **(c₂)** κ (I_G/I_D-vs-τ), and **(d₂)** β (b-vs-τ), **(e₂)** λ (L-vs-τ) on $c(CO_2)$.

Table A2. The overall trends of residence time influence on the SWCNT parameters at different CO_2 concentrations (numbers of arrows qualitatively illustrate evolution rates with τ (parameter n was calculated using equation (4), while the other ones are derived from fitting the results).

c(CO_2)	r (R_{90})	γ (Yield)	λ (length)	β (bundling)	κ (I_G/I_D)	n (concentration)
0.00	2.22 ± 0.29	1.75 ± 0.71	0.41 ± 0.04	0.19 ± 0.05	0.55 ± 0.37	-1.10 ± 0.06
0.37	1.64 ± 0.26	1.90 ± 0.64	0.31 ± 0.11	0.09 ± 0.23	0.74 ± 0.15	-1.25 ± 0.23
0.74	1.13 ± 0.40	1.67 ± 0.21	0.21 ± 0.05	0.09 ± 0.01	1.07 ± 0.29	-1.31 ± 0.03
1.49	0.008 ± 0.16	0.97 ± 0.35	0.03 ± 0.02	0.08 ± 0.08	0.08 ± 0.18	-1.40 ± 0.08
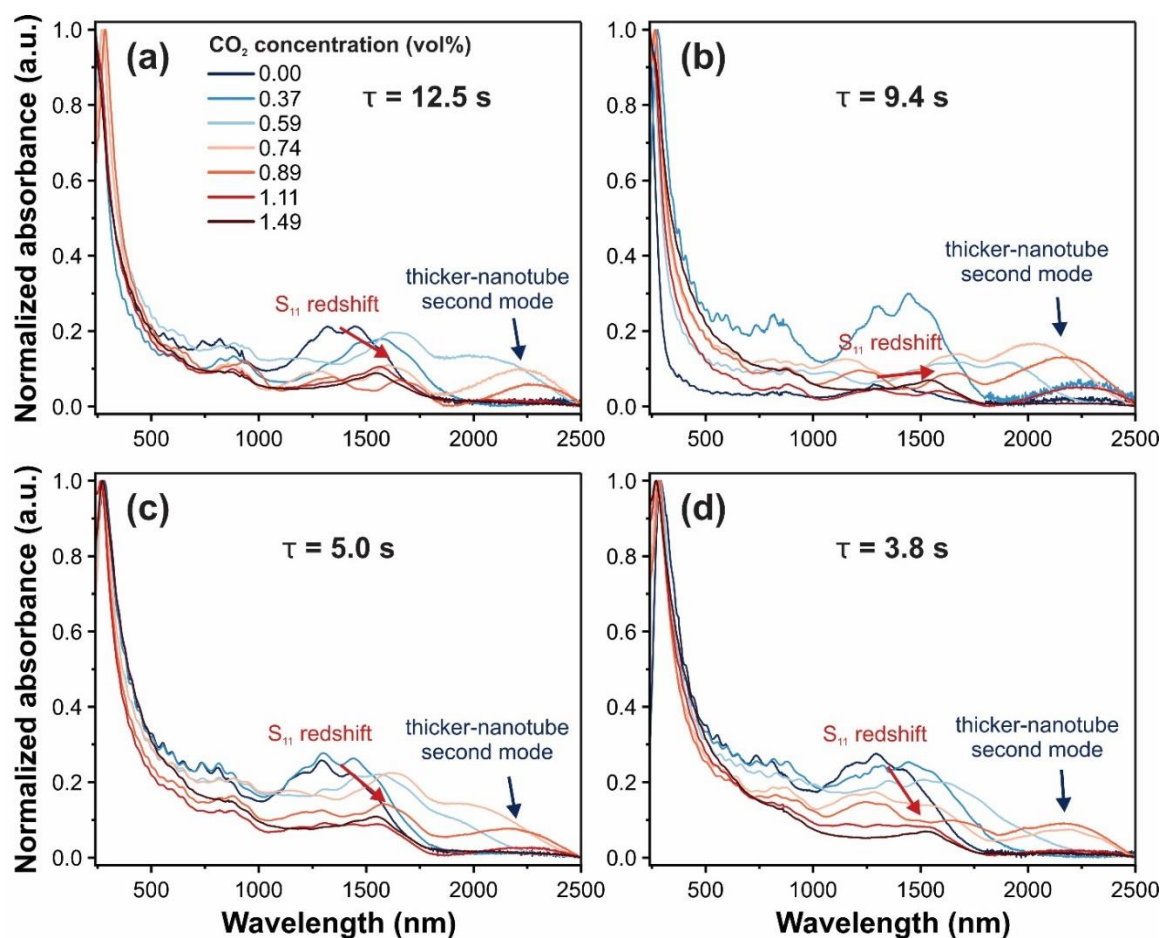
Figure A8. UV-vis-NIR spectra of the SWCNT films synthesized at 880 °C at different c(CO_2) (shown in the legend) and at different residence times: **(a)** 12.5 s, **(b)** 9.5 s, **(c)** 5.0 s, **(d)** 3.8 s with the highlighted S_{11} redshift and the formation of the second mode of thicker SWCNTs.